Diploma thesis

Catalysis of aldol condensations and hydrogenations in flow conditions using (Cu:)Mg:Al oxides

Carried out at the

Institute of Materials Chemistry
TU Wien

under supervision of

Associate Prof. Dr.in techn. Karin Föttinger
and Alberto Tampieri, PhD

by

Alexander Eder

November 19, 2024

Abstract

Aldol condensation and subsequent hydrogenation is a reaction pathway relevant for transforming biomass feedstock into usable fuel. Hydrotalcites are versatile solid bases, whose catalytic properties can be fine-tuned by changing elemental composition, calcination into mixed metal oxides and rehydration. Herein, the viability of hydrotalcite-derived catalysts was researched for aldol condensation and reduction with H_2 using a model system of benzaldehyde and acetone. Preliminary tests were done in a batch reactor testing the catalytic performance of different hydroxide and oxide catalysts. It was found that while being effective in producing benzylideneacetone, even more so when previously rehydrated (increasing both conversion and yield of benzylideneacetone), mixed metal oxide catalysts deactivate $< 24\,\mathrm{h}$ in flow conditions. Flushing acetone or calcination at 450 °C did not prove effective in restoring the activity of the catalysts. The use as hydrogenation catalysts was studied using 1:1:1 Cu:Mg:Al and 0.2:1.8:1 Cu:Mg:Al mixed metal oxides. Using a model system of benzylideneacetone in isopropanol, complete and selective conversion to 4-phenyl-2-butanol was achieved already at 50 °C. Furfurylideneacetone showed similar results, but minimally less selectivity. It was shown that pre-treatment of those catalysts (rehydration, reduction) can be performed in-situ inside a flow reactor. Those findings indicate promising use cases for hydrotalcite-based materials, especially for the use as hydrogenation catalyst. Further studies can use the results as a starting point for optimizing the reaction and elucidate the mechanism of catalyst interaction and deactivation which can deepen our general understanding of heterogeneous catalysis.

Kurzfassung

Aldolkondensation und nachfolgende Hydrierung sind weitgenutzte Transformationen, um Biomasse in wertvolle Kraftstoffe zu verwandeln. Hydrotalkit ist ein Mineral, das als heterogener basischer Katalysator verwendet und in weitem Maße durch Modifikationen der chemischen Zusammensetzung, durch Kalzinierung und Rehydrierung an die Bedürfnisse der Reaktion angepasst werden kann. In dieser Arbeit wurden verschiedene Feststoffe auf Hydrotalkitbasis auf ihre Eignung als Katalysator für Aldolkondensationen und Reduktionen mit H_2 anhand eines Modellsystems aus Benzaldehyd und Aceton untersucht. Erste Tests wurden in einem Batch-Reaktor durchgeführt, um verschiedene Oxide und Hydroxide zu vergleichen. In den folgenden Flowreaktionen wurde herausgefunden, dass 2:1 Mg:Al Oxid effektiv Benzylidenaceton herstellen kann. Dies wird durch Rehydrierung weiter verbessert, sowohl der maximale Umsatz, als auch die maximale Ausbeute an Benzylidenaceton steigern sich. Allerdings deaktiviert der Katalysator in beiden Fällen innerhalb von 24 h. Spülen des Reaktors mit Aceton oder erneute Kalzinierung bei 450 °C erwies sich beides als ineffektiv, um die katalytische Aktivität wiederherzustellen. Die Verwendung als Katalysator für Hydrierungen wurde anhand gemischter 1:1:1 Cu:Mg:Al sowie 0.2:1.8:1 Cu:Mg:Al Oxide untersucht. Anhand eines Modellsystems aus Benzylidenaceton in Isopropanol wurde festgestellt, dass bereits bei 50 °C vollständiger und selektiver Umsatz zu 4-Phenyl-2-butanol erzielt werden kann. Untersuchungen mit Furfurylidenaceton zeigen ähnliche Ergebnisse, wenn auch etwas geringere

Selektivität. Weiters wurde gezeigt, dass Vorbehandlungen (Rehydrierungen, Reduktionen) erfolgreich in-situ durchgeführt werden können. Diese Ergebnisse zeigen das Potential für Hydrotalkit-basierte Materialien auf, vor allem in Bezug auf Reduktionen. Für zukünftige Studien können die Resultate als Ausgangspunkt für die Optimierung der Reaktionen dienen. Im Hinblick auf wissenschaftliche Grundlagenforschung bieten sie außerdem eine Möglichkeit, bei der Aufklärung der Reaktions- und Deaktivierungsmechanismen von heterogenen Katalysatoren zu unterstützen.

Contents

1 Indexes

1.1 List of Symbols

b ..... Slope of calibration curve
eq ..... Equivalents / 1
g ..... Standard gravity / $9.80665\,\mathrm{m\,s^{-2}}$
m ..... Mass / kg
M ..... Molar mass / $\mathrm{kg\,mol^{-1}}$
n ..... Amount / mol
s ..... Standard deviation
V ..... Volume / L

1.2 List of Abbreviations

BET ..... Brunauer-Emmett-Teller
DI ..... Deionized
FID ..... Flame ionization detector
GC ..... Gas chromatograph(y)
HPLC ..... High performance liquid chromatography
IR ..... Infrared
LOD ..... Limit of detection
LOQ ..... Limit of quantitation
NMR ..... Nuclear magnetic resonance
RT ..... Room temperature
SEM ..... Scanning electron microscope
TCD ..... Thermal conductivity detector
TPR ..... Temperature programmed reduction
UV ..... Ultra violet
XPS ..... X-ray photoelectron spectroscopy
XRD ..... X-ray diffraction

Abbreviations of chemicals

BZ ..... Benzaldehyde
BZcon ..... Benzylideneacetone
Cu-MMO .. Cu:Mg:Al oxides
DAA ..... Diacetone alcohol
dba ..... Dibenzylideneacetone
DCM ..... Dichloromethane
EtOH ..... Ethanol
Fcon ..... Furfurylideneacetone
F2con ..... Difurfurylideneacetone
hBN ..... hexagonal boronitride
HMF ..... Hydroxymethylfurfural

iPrOH ..... Isopropanol
MES ..... Mesityl oxide
MMO ..... Mixed metal oxide
MX ..... Meixnerite-like structure
PTFE ..... Polytetrafluoroethylene
PVC ..... Polyvinyl chloride

2 Introduction

2.1 Motivation

At the current point of time, both energy as well as many chemicals are produced from resources such as petroleum, as fossil fuels proved to be the main feedstock during the last decades. However, concerns about the rising CO_2 levels in our atmosphere and the connected climatic changes mandate the search for greener alternatives. One of those alternatives could be the use of biomass as a chemical feedstock. As long as no fossil fuels are used throughout the production chain, they are net-zero regarding CO_2 emissions, as carbon is consumed from the environment during the growth of said biomass. [1]

Because of its widespread use, the refining of fossil fuels has been thoroughly optimized over the last few decades. For the refining of biomass, this process is still in an earlier stage and cost is still a prohibitive factor that impedes the implementation on a wide industrial scale. However, it has been predicted, that the shift more and more towards bio-based feedstocks is already under way. [1]

Processing those involves multiple steps and can go along various pathways. One would be manufacturing chemicals that are equivalent to the derivatives from mineral oil through biomass gasification to syngas and downstream Fischer-Tropsch or methanol production units. Another option would be pyrolysis and liquefaction of the biological matter and further refining of those so called "bio-oils" towards fuels. The conversion of biomass to sugars through fermentation on the other hand is the first step to either further fermentation towards ethanol or dehydration towards alkanes. [1]

For this last option a promising process for production of fuels and starting materials for the chemical industry has already been established. Increase in the length of carbon chains can be achieved by aldol condensation. The products, usually highly unsaturated carbohydrates, can then be converted into alkanes by subsequent hydrogenation and dehydration steps [2].

Often those reactions, especially H_2 treatment, involve expensive precious metals like Pt or Pd. [1]

In contrast to the petrochemical industry, many methods for the refining of biomass do not yet use heterogeneous catalysts. [1] HT and HT derived materials have already been researched for the past 40 years as such catalysts. [3, 4] Previous findings have pointed out, that while the material is highly active, especially in its rehydrated form, it suffers from technical difficulties like deactivation of catalytically active centers in contact with air and lack of reusability. Combined with the low cost of their alternative, aqueous bases like NaOH, the use of this type of catalyst has so far been not attractive for production purposes. [5]

This study therefore aims to aid the understanding of HT-based catalysts, focusing on their use in aldol condensations under flow conditions. As a second target the investigation of HT modified with Cu was chosen and their use as hydrogenation catalysts in flow reactions. It is proposed that better understanding of those reactions

can help in the development of reactions using biomass-derived molecules for the production of bio-based fuels and the design of the respective catalysts. The focus here lies on industrial production of bulk chemicals, for which it will be interesting implementing continuous processes.

2.2 Examined reactions

2.2.1 Aldol condensation

The aldol condensation is a commonly used organic reaction for creating new carbon-carbon bonds. This can either be a double bond or a single bond in case the reaction is incomplete, then called aldol reaction. Below in Figure 1, exemplary an aldol condensation between an aldehyde and a ketone is shown. [6]

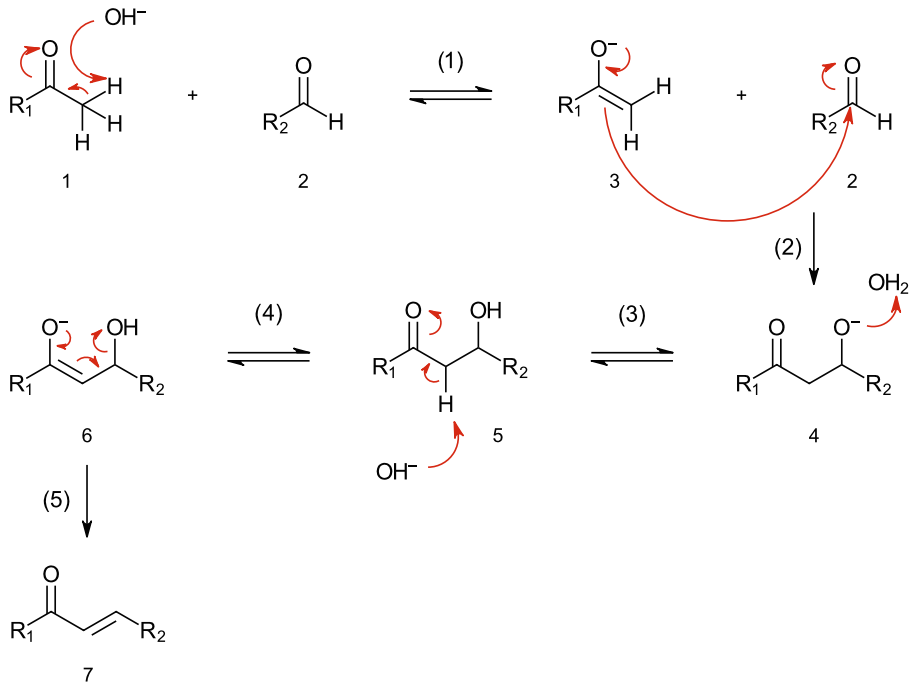

Figure 1: Mechanism of aldol condensation pictured as base-catalyzed reaction of an aldehyde and a ketone. [6]

It can be described in 5 major steps: (1) Enolization, (2) nucleophilic addition, (3) acid-base equilibrium, (4) enolization, (5) elimination. This last dehydration step (5) was found to be the rate-limiting step. [6]

When catalyzed by heterogeneous catalysts with basic sites it is likely that the reaction takes place after the aldehyde as well as the ketone adsorb on the surface of the catalyst as has been studied in similar reactions. The keton is suggested to be adsorbed as a carbanion in this step. [7] When heterogeneous catalysts that have OH^- sites are used, it was also proposed that those are the main active sites similar to the classic mechanism described in Figure 1. [3]

For the purpose of heterogeneous catalysis for example BaO, SrO, CaO or MgO have shown activity. [8]

Figure 2 shows the reaction scheme of the investigated aldol condensation between acetone and BZ. This well-known reaction in its base-catalyzed form has already been studied for over 100 years. [9]

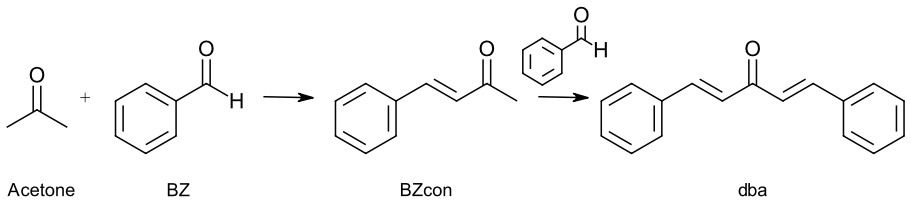

Figure 2: Reaction scheme of the aldol condensation between BZ and acetone performed in this work with the used abbreviations.

Traditionally such reactions are carried out using NaOH or KOH [10], but even solvent-free mechanochemical approaches have been successfully tried, griding the starting materials together with a base catalyst. [11] Grapheneoxides have also proven to be active in catalyzing this reaction. [12]

It is also possible to perform this reaction without any catalyst, as was shown under high-pressure conditions by heating the reactants in liquid water at 250 °C for 5 h, achieving a yield of 24 %. [13]

Recently, the push for greener alternatives to liquid bases has renewed the interest and incentivized research on solid bases as catalysts for the aldol condensation of BZ and acetone. [14, 15, 16]

Previous works have already shown that this reaction can be effectively catalyzed by Mg:Al HT based materials. [4, 17] Performing the reaction in another solvent instead of neat in acetone lowers the effectiveness. As for the constitution of the catalyst, a 2:1 Mg:Al ratio seems to be optimal for catalysis of the aldol reaction. [18].

2.2.2 Hydrogenation reaction

Hydrogenations can be carried out in various different ways, for example through using hydride donors, homogeneous hydrogenation using metal complexes or heterogeneous catalysts using H_2 as donor. [19]

Almost 10 % of reactions performed in pharmaceutical research and development involve a reduction and about half of those are direct hydrogenation reactions using precious metals as catalyst. It is often desirable to perform reductions through hydrogenation because of the high atom efficiency of this reaction. [20]

For hydrogenations it is especially beneficial to implement them as flow processes in liquid phase as the reactor will then be mostly filled by liquid and the amount of H_2 can be kept to a minimum, increasing the safety of the process. [21]

Greater availability and lower price have turned the attention towards non-noble metals such as Ni, Co, Fe or Cu. [22] Supported copper nanoparticles have previously been shown to be effective in flow hydrogenations being able to achieve complete

conversion over multiple days, for example for the reduction of nitro groups to amines. [23]

Earlier work has already proven that supported Cu can achieve selective and complete conversions in hydrogenations under flow condition while being stable for a prolonged time under conditions close to industrial use (for example propyne to propene for 1 month using a Cu/SiO_2 system [24]) A similar reaction has been performed using Cu:Al hydrotalcites. [25] Cu/Al_2O_3 systems have been used for hydrogenation of HMF using methanol as a solvent. [26]

Mechanistically, it is usually necessary for H_2 to dissociate for heterogeneous hydrogenation because H_2 can not bind sufficiently strong to the surface of metals. While many noble metals do adsorb H strong enough, other materials like Cu are reliant on the presence of surface defects for their activity. Once adsorbed, hydrogen can diffuse over the surface easily. [19]

Studies have shown that simple α,β-unsaturated aldehydes preferably adsorb via the C=C double bond. However, as molecules get larger and more complex, those binding energies are influenced more by the substituents which can go as far as only binding via the carbonyl being stable. This kind of studies however were usually performed on single crystals and do not account for the increased complexity of supported systems. [19]

In Figure 3 as an example the reduction to the alcohol with alkane side chains is shown, which is the main product of the investigated reactions. In this case, many more products (no reduction of the double bond or carbonyl, further decomposition) can potentially form.

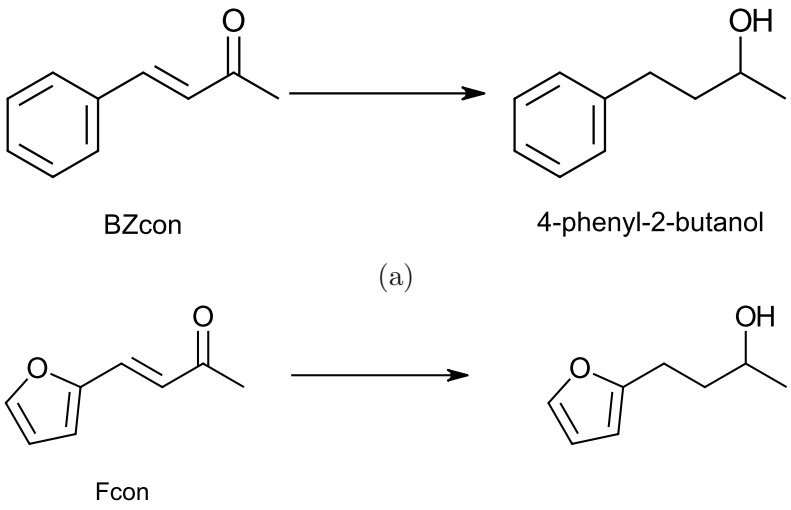

Figure 3: Exemplary reaction scheme of the hydrogenation of (a) BZcon and (b) Fcon with the used abbreviations.

As previously mentioned, there are multiple methods to hydrogenate compounds and many of them have already been tried in the reduction of BZcon and Fcon.

One of those methods more applicable in the laboratory scale in organic synthesis uses the help of metal-organic complexes. For example, iridium diphosphine complexes have been used to selectively reduce the carbonyl [27], or ruthenium complexes to selectively reduce the carbon-carbon double bond. [28]

Also electrochemical reduction methods of BZcon have been researched. On mercury electrodes, mechanistical studies found out that the reduction to 4-phenyl-2-butanol happens in two steps, the reduction of the double bond and the carbonyl [29].

Multiple studies report that the reduction of BZcon is pH dependent and in aqueous solutions a neutral pH is desirable. [29, 28]

Another relevant group of catalysis is the hydrogenation over supported metals. Research on commercial supported Ni catalysts was able to show that the H_2 pressure does not influence the selectivity of the catalyst, but can accelerate reaching the equilibrium. [18]

Hydrogenation also have been performed on furfural-derived materials. In the context of fuel production the further reduction F2con to alkanes with Raney-Ni and supported Pt catalysts has been studied. [30, 31] However, for furfural-based chemicals the existence of different type of double-bonds together with an oxygen atom in the ring seems to make optimization of the hydrogenation conditions more difficult. [30]

Cu has also been reported to selectively reduce the carbon-carbon double bound of Fcon when deposited on Al_2O_3. [32]

2.3 Hydrotalcite-derived materials

2.3.1 Hydrotalcite structure

Hydrotalcites fall in the general category of double layered hydroxides (LDH). They can be described by the formula $(M_{1\text{-}x}{}^{2+}M_{1\text{-}x}{}^{3+}(OH)_2)^{x+}(A_{x/m}{}^{m-}) \cdot n\,H_2O$ $(0.25 < x < 0.33)$. For the cations (divalent $Mg^{2+}, Ca^{2+}, Zn^{2+}, Ni^{2+}$, trivalent most commonly $Al^{3+}, Fe^{3+}, Cr^{3+}$) as well for the anions ($OH^-, Cl^-, NO_3{}^-, CO_3{}^{2-}, SO_4{}^{2-}$) multiple options are possible. Those ions are split into two types of layers, one negatively charged, the other positively. The latter has a structure similar to brucite with the formula $(M_{1\text{-}x}{}^{2+}M_{1\text{-}x}{}^{3+}(OH)_2)^{x+}$, while the other one contains the counter anions as well as the interlayer water. [4]

Anion exchange can be achieved by suspending the HT in a solution that contains the target anion and heating the solution. [4] HT containing Mg and Al as cations is a naturally occurring material. [33]

The material also contains some acidic sites, although they are regarded to be too weak to be responsible for the catalysis of condensation reactions. They could, however, be responsible for some of the activity in the dehydration step (see step (5) in Figure 1). [4]

2.3.2 Mixed metal oxide structure

MMO material has more and stronger basic sites than HT. It was speculated that this is caused by inhibition of basic sites by water molecules. Activation of Mg:Al HT by calcination at 450 °C was already previously described, while calcination at lower or higher temperatures led to loss of activity. [3]

Under those treatment conditions less stable carbonates are removed, but those with high thermal stability persist. When performing the calcination at temperatures high enough for removal of hydroxyl groups, but low enough to prevent formation of spinels, also loss of activity occurs. Most basic sites of the MMO calcined at 450 °C are therefore attributed to hydroxyl groups. [4]

This calcined material is known to have a lamellar structure. [34] Stored in air, the already calcined material can suffer a loss of activity. This is attributed to uptake of CO_2 from the atmosphere. [4]

The general structure of those mixed oxides resembles that of MgO, just with smaller lattice parameters because of the presence of Al, which has a smaller ionic radius than Mg. [34]

2.3.3 Meixnerite-like structures

A so-called memory effect is observed with those type of materials. After calcining HT into MMO, the structural change can be reverted by exposing the material to water, restoring the layered structure. [35]

Rehydration of the catalyst can improve the reaction rate of condensations reactions. Since this is counterintuitive to the stronger basicity of the MMO catalyst, it was proposed that the mechanism of condensation is preferably catalyzed by OH^-. [3]

This rehydrated structure containing no more carbonates can also be called a meixnerite-like structure [34], leading to the here used abbreviation MX. While longer rehydration is able to further improve the catalytic activity of the material, the returns regarding the time diminish after a rehydration time of about 3 h. [3]

Exchanging the anions and then calcining is a possibility to fine-tune the properties of the catalyst. It was found that HT exchanged to contain carbonates or acetates and then calcined is more basic and shows better activity for aldol condensations (of furfural and acetone) than those containing nitrates. [36] Presence of even small amounts of Cl^- seems to be particularly inhibiting to the catalysis of aldol condensations. [3]

The rehydration can be performed both in the liquid and the vapor phase with similar results. [34]

2.4 Flow chemistry

Cost savings from automation, safety concerns, advantages for manufacturing and a paradigm shift to greener methodologies drive the switch to continuous flow processing in the chemical industry. [21, 37]

Sectors manufacturing more complicated molecules like the fine chemical or pharmaceutical industry inherently produce significantly more waste per product than those producing bulk chemicals. [38] Those sectors have the potential to benefit considerably from the implementation of flow processes. [21]

They allow for performing reactions in a highly controlled environment, benefiting from increased mixing, high rate of heat exchange, control over the contact time and more exact adjustment of temperatures. While those measures can help to improve the yields of a reaction, at the same time flow processes allow for advanced in-line analytics to monitor the operation and ensure product quality already at the point of production. [21]

Also due to the usually smaller reactor volumes compared to batch products, it is possible to implement reaction conditions (temperature, pressure) to speed up a reaction that would otherwise not be feasible. This is also true from a safety point of view, also considering that potentially forming dangerous or unstable intermediates will be rapidly consumed and their build-up prevented. Ease of removal of permanent gases is another advantage that should be considered. [21]

On the other hand, another aspect that has to be considered when designing flow processes is that ideally not only the reaction, but also the purification can be performed continuously, which complicates planning. Recovery and reuse of unreacted reagents and solvent is another possibility to increase efficiency of flow reactions. [39] It should be noted that optimizing some reaction parameters may lead to problems downstream, therefore the whole process should always be taken into consideration during process design. [21]

There are various schemes for experimental design described that can help with this. For creating an optimal process, design of experiments guidelines (DoE) can provide assistance. [37]

In this framework, first clear and achievable objectives have to be defined, where the already available information has to be taken into consideration as well as the overall project goal (for example optimization for purpose of yield, minimizing waste, etc.). It might be necessary to perform more extensive screening experiments to survey the behavior of reactions when changing certain parameters when the work is done on reactions that are either novel in general or simply not well described in literature. [37]

An initial screening is also instrumental in obtaining information about what change of parameters will generate the highest response. Then, by careful choice of parameters, the number of experiments can be minimized while simultaneously guaranteeing insight over a larger section of the experimental space compared to when only changing one variable at the time. [37]

Flow reactors are especially suitable for this type of experiments, as the high possible degree of automation of the reactor as well as quick reaching of an equilibrium state allows for effective cycling through a high number of conditions, assisted by the possibility of in-line analytics. [37]

However, since this study focuses on the exploration of conceptual ideas over optimization of processes, a more traditional approach to experimental design was chosen.

2.5 Catalysis

2.5.1 Catalyst deactivation

For liquid phase flow aldol condensations of furfural with ketones catalyzed by solid bases (supported MgO and CaO) a major contributor to catalyst deactivation was found to be the formation of organic acids through Cannizzaro reaction of the aldehyde. This was found under exclusion of other possible sources of deactivation for this catalyst like influence of CO_2, H_2O or impurities of the feed. [40]

Regarding the gas-phase aldol condensation of acetone adsorption of oligomers was found to be a deciding factor in the deactivation of MgO as solid-base catalyst before the formation of coke. [41]

2.5.2 Heterogeneous catalysis

For reactions to be catalyzed through a heterogeneous catalysts, it is generally necessary for the reactants to absorb on the catalysts surface. Multiple mechanisms have been identified. Two important ones are Langmuir-Hinshelwood and Eley-Rideal, which are schematically depicted in Figure 4. [19]

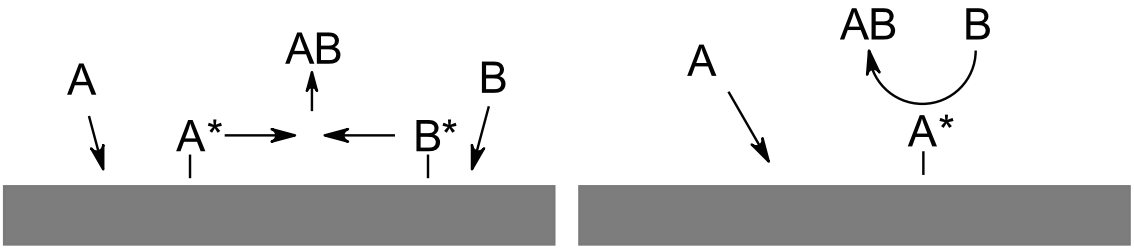

Figure 4: Schematic drawings of the (a) Langmuir-Hinshelwood and (b) Eley-Rideal mechanism. * denotes an adsorbed/absorbed species. Adapted from [19, p. 422].

Some hydrogenation reactions using Cu were speculated to follow an Eley-Rideal mechanism, however, this has not been fully proven. Meanwhile Langmuir-Hinshelwood remains relevant for all kinds of heterogeneously catalyzed reactions, where the reaction only takes place after thermal equilibration between all involved reactants and the surface has been reached. [19]

3 Results and Discussion

3.1 Hydrotalcite-based mixed metal oxide catalysts

3.1.1 Influence of catalyst preparation on morphology and catalytic activity

It was hypothesized that the standard coprecipitation method described in section 6.5.1 could be substituted by an easier and less time-consuming method of precipitation without significant change in catalyst structure and activity.

As method of choice the same solutions as described in section 6.5.1 were prepared, but instead of adding the metal nitrate solution (2:1 Mg:Al) dropwise, the base solution was added quickly via syringe until a pH of about 11 was reached (checked by pH-paper). Then, the white precipitate was collected and washed by centrifugation, dried and further calcined to a MMO as usual.

It can be seen in Figure 5 that the HT prepared by the fast method had a translucent appearance (after drying, before calcination to MMO) instead of being a dull powder. Also, it was harder and more brittle than the one prepared using the standard method.

(a) (b)

Figure 5: Pictures of 2:1 Mg:Al HT that was prepared using the (a) standard method (b) fast method.

Table 1: BET surface area of 2:1 Mg:Al MMO prepared using the standard and fast method.

Sample	BET surface area / $m^2\,g^{-1}$
MMO standard method	236
MMO fast method	188

BET surface area was measured for both materials, with the MMO prepared by the standard method showing greater surface area as reported in Table 1. Figure

6 shows the respective physisorption isotherms. According to the IUPAC definition [42] the shape of both can be classified as Type IV(a), suggesting a mesoporous material with pores $> 4\,\mathrm{nm}$.

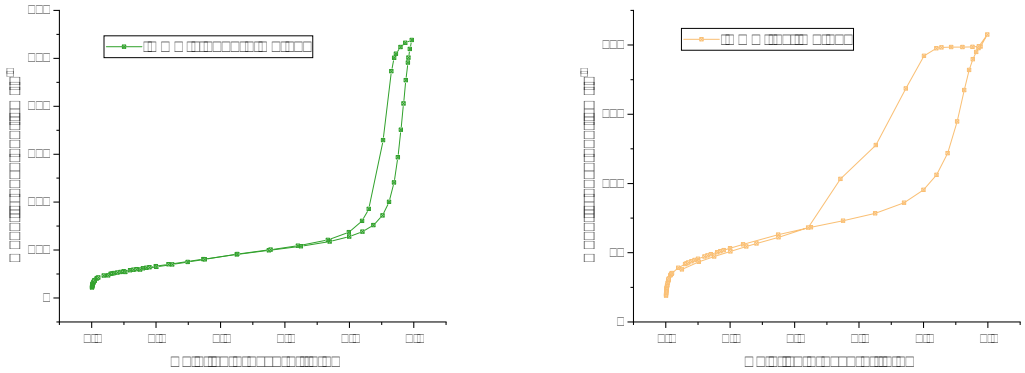

(a) (b)

Figure 6: Adsorption/desorption isotherms of 2:1 Mg:Al MMO that was prepared using the (a) standard method (b) fast method.

Figure 7 shows that also on a microscopic level differences can be seen: While the MMO prepared using the standard method shows fine lamella structures upon closer examination, no such structure could be found on the fast-prepared MMO. This could also be a possible explanation for the lower surface area of the latter.

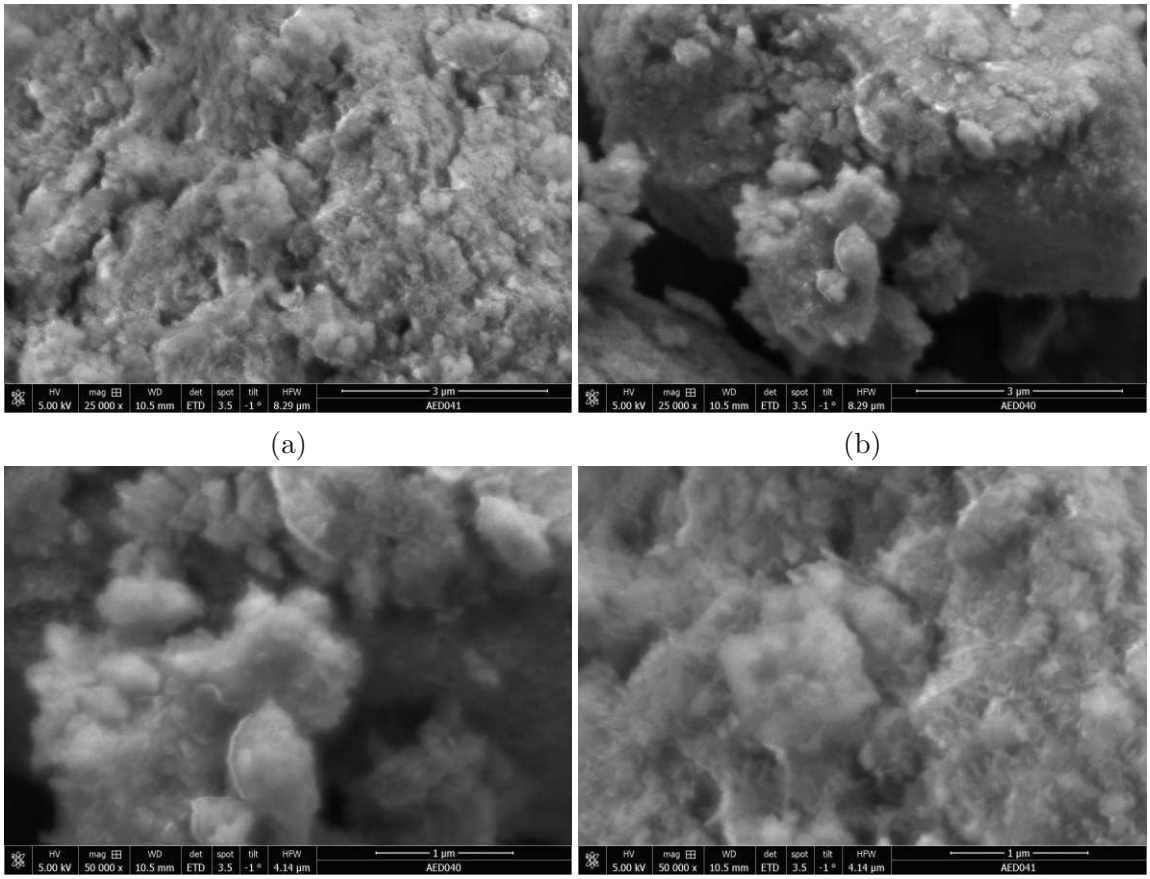

(a) (b)

(c) (d)

Figure 7: Recorded SEM images of 2:1 Mg:Al MMO that was prepared using the standard method at 25 000 x magnification (a) and 50 000 x magnification (c) as well as the fast method at 25 000 x magnification (b) and 50 000 x magnification (d). Poor resolution and white spots seen in the image are resulting from charging of the samples.

Table 2: Results of batch catalytic tests (50 °C, 4 h) comparing 2:1 Mg:Al MMO synthesized using the standard method and using the fast method.

	MMO standard	MMO fast
Conversion BZ / %	18	12
Yield BZcon / %	9	5
Area% Bzcon / %	70	61
Area% unknown / %	22	24
Area% dba / %	8	15
concentration DAA / mmol mL^{-1}	0.019	< LOQ (0.013)
concentration MES / mmol mL^{-1}	< LOD (0.0030)	< LOD (0.0026)

Both materials were compared in a batch reaction with acetone and BZ as starting materials. The results summarized in Table 2 show that the activity of the catalyst

synthesized using the standard method achieved about 50 % higher yields for all products.

This combined evidence lead to the rejection of the initial hypothesis. It was not possible to conclude that the faster method of synthesis will yield equal results as the slow coprecipitation and therefore the slow method was continued to be used.

3.1.2 Stability

The stability of MMO catalysts when stored was examined to research the necessity of inert storage conditions or a pre-treatment of the catalysts before use since those catalysts are susceptible to deactivation by uptake of CO_2 from the air (see also chapter 2.3.2). [4]

MMO samples stored in two different ways were measured via XRD. One sample was stored in a vial inside a cabinet, the others were stored in a crucible only covered by aluminum foil. The storage time was comparable, with 15 d for the vial sample and 23 d for the crucible sample.

The diffractograms depicted in Figure 8 show that the sample in the vial retained the MMO structure, while the samples stored in the crucible partially reconstructed into an HT. The XRD data shows both signals from MMO structure as well as from HT structure, which means that while there are significant changes to the bulk material, it has not (yet) fully reconstructed to the HT.

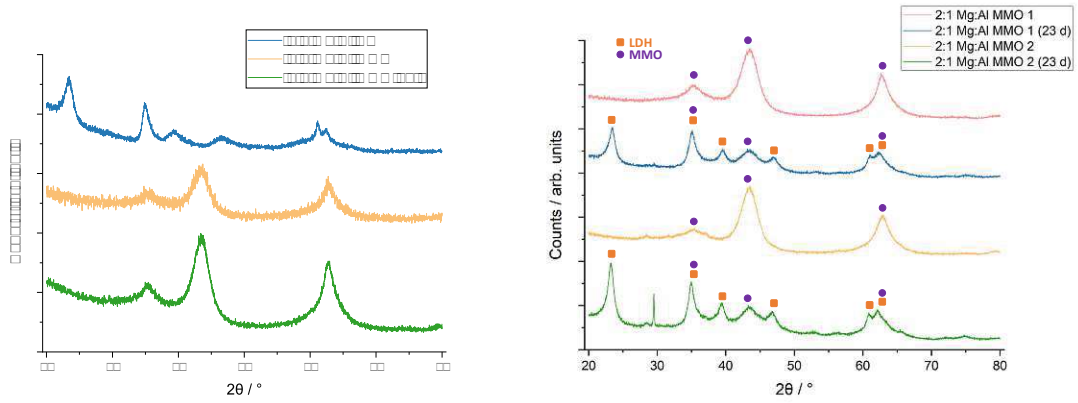

(a) (b)

Figure 8: (a) Diffractograms of 2:1 Mg:Al HT, MMO after calcination and MMO after storage in a closed vial after 15 d. (b) Diffractograms of 2:1 Mg:Al MMO after calcination and after being stored in an unsealed crucible for 23 d. Reflections belonging to HT and MMO phases are assigned.

Table 3: BET surface area of different 2:1 Mg:Al MMO samples. The first ("fresh") sample was taken immediately after calcination, the second ("stored") after being stored in an unsealed crucible for 22 d.

Sample	BET surface area fresh / $m^2\,g^{-1}$	BET surface area stored/ $m^2\,g^{-1}$
1	188	24
2	236	48

The results of the BET surface area measurements shown in Table 3 also support changes of the stored material. The surface area of the partially reformed HT is significantly lower by a factor of 5-8. Figure 6 shows the respective physisorption isotherms. Compared to the isotherms of the freshly calcined material depicted in Figure 6 the hysteresis is less pronounced, indicating a change in the pore structure. This also means that the BET surface area will be less reliable as there is no distinct Point B in the isotherms. [42]

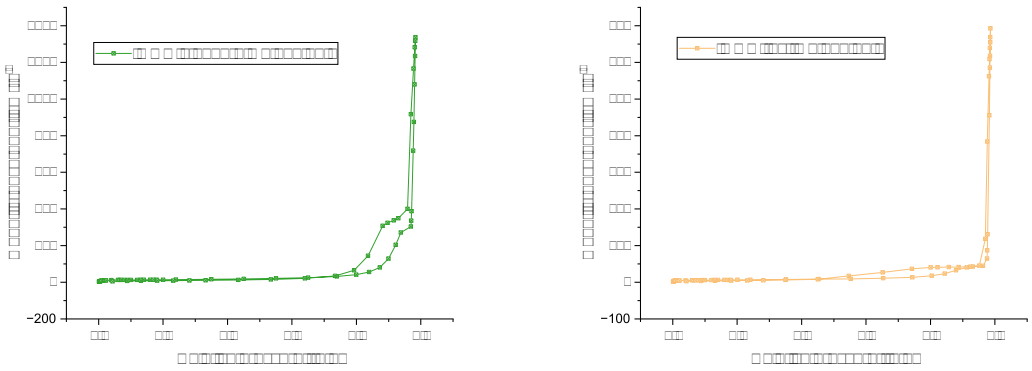

(a) (b)

Figure 9: Adsorption/desorption isotherms of different 2:1 Mg:Al MMO samples after being stored in an unsealed crucible for 22 d. (a) Standard preparation method. (b) Fast preparation method.

Visually, changes were also noticed. As shown in Figure 10, when leaving initially colored Cu-MMO (green before reduction, black after reduction) exposed to air for a prolonged timespan, their color reverted back to that of the HT (light blue).

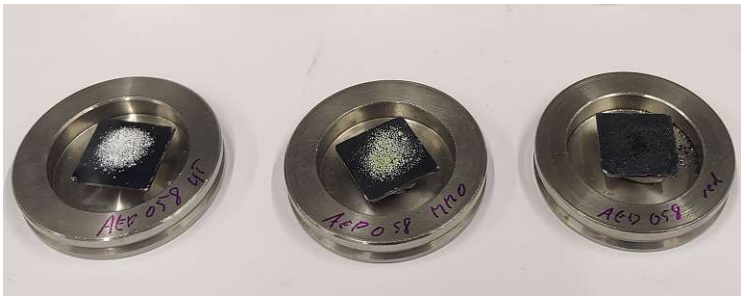

(a)

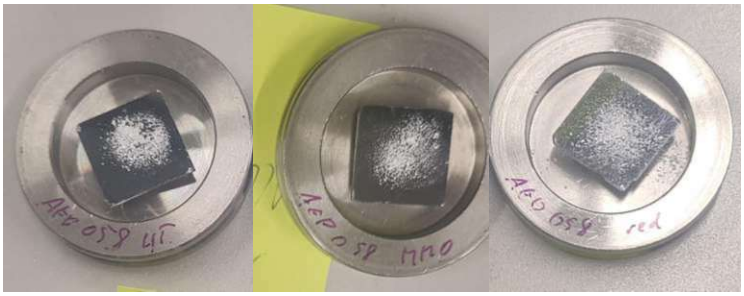

(b)

Figure 10: Pictures of Cu-MMO (a) before and (b) after being exposed to air for 12 d.

To determine the length of calcination that will be necessary to revert changes that occured over storage during production of MMO a sample was taken after 30 min and 4 h of calcination each. The XRD results can be seen in Figure 11 and indicate that after 30 min the majority of material already was converted, only the ratio of the reflections at around 35° and 43° is not right. Both materials show a reflection at 35°, but the one of the HT is higher. Therefore a shifted ratio towards a higher reflection at 35° means that there are still underlying signals from the starting material. Since other HT reflections are not visible, it was concluded that only a minor part of the material was still in HT form. After 4 h, the transformation is already completed.

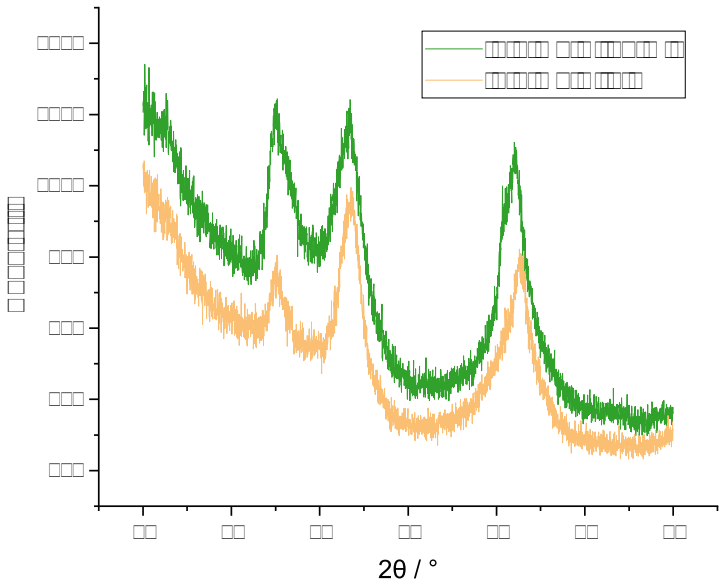

Figure 11: Diffractograms of 2:1 Mg:Al after 30 min and 4 h of calcination at 450 °C in a muffle furnace.

The presented data shows that it is necessary to store MMO catalysts under inert conditions or perform a calcination directly before use. Even in air, the bulk material seems to have some stability. However, since the surface of the material will be the first to undergo changes it is possible that deactivation happens even faster than the evidence collected shows. Since the catalytic reactions would also take part on the surface it was determined that the best possible method to ensure full activity of the material would be to perform a short calcination before catalytic tests. A 30 min calcination was deemed sufficient.

3.1.3 Rehydration experiments

In-situ rehydration of the 2:1 Mg:Al catalyst was performed by flowing pure water for 30 min after the pre-treatment and then flushing the reactor again with O_2 to avoid contact of water and reaction solvent.

As the XRD data in Figure 12 shows, the rehydration was successful and led to formation of a material that was a mixture of HT and MMO.

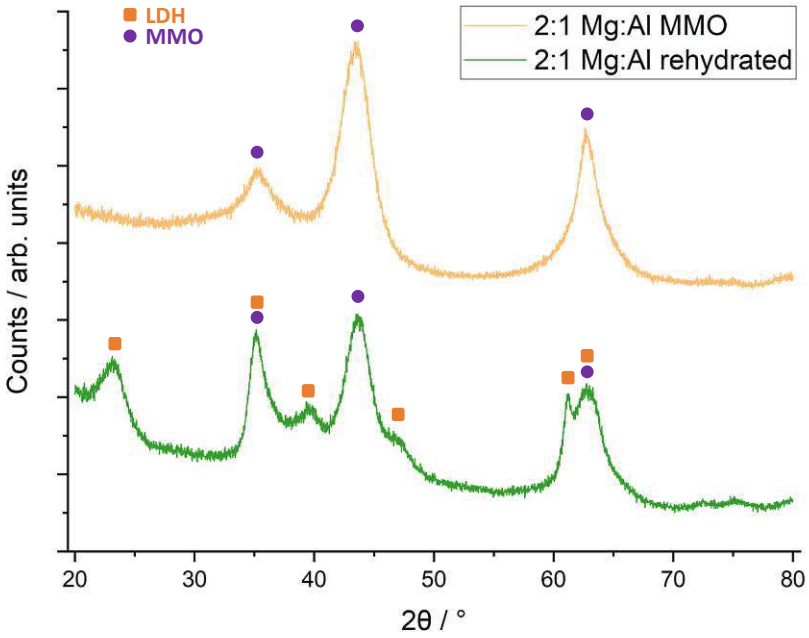

Figure 12: Diffractograms of 2:1 Mg:Al MMO before and after in-situ rehydration during a flow reaction. HT and MMO phases are annotated in the diffractograms.

Those results were obtained after completion of the reaction flowing acetone and BZ, which indicates some stability of the reconstructed material. However, some changes during the reaction (for example further rehydration through condensation water) cannot be excluded by this measurement and need further research.

Rehydrations on MgO material with deposited Al (through calcination of MgO in a aluminum isopropoxide solution, provided by research group of David Kubička, Department of Sustainable Fuels and Green Chemistry, UCT Prague) were performed to study the influence of the Al content on the characteristics of the material. It was observed that material with higher content of Mg resulted in a more liquid product after centrifugation, while those with higher surface Al content yielded flaky, aggregated solids. Moreover, the rehydrated material got increasingly more brown after rehydration with lower content of Al.

XRD were measured of the rehydrated and dried samples. In Figure 13 it can be seen that with decreasing Al loading less of LDH phase is reformed and instead more $Mg(OH)_2$ formed.

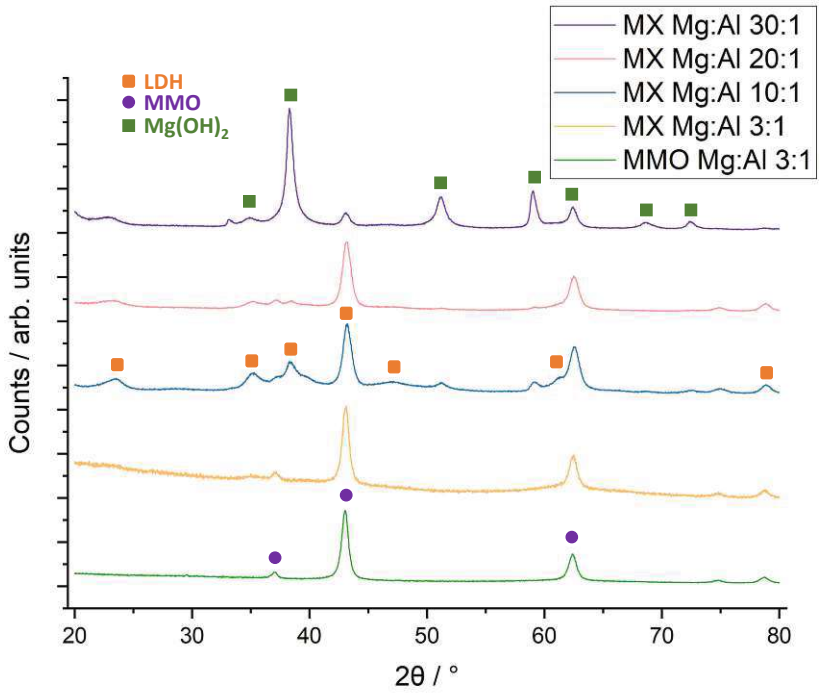

Figure 13: Diffractograms of rehydrated and dried samples after rehydration for 20 min at RT. $Mg(OH)_2$, HT and MgO phases were assigned exemplarily on the diffractograms that showed the reflections most clearly.

This corresponds to the physical changes mentioned above. All HT and MMO diffractograms just showed the MgO pattern of the bulk material. Exemplarily, the MMO of the Mg:Al 3:1 sample is shown. The diffractograms of the provided reference samples of a Mg:Al sample prepared by coprecipitation are shown in Figure 14.

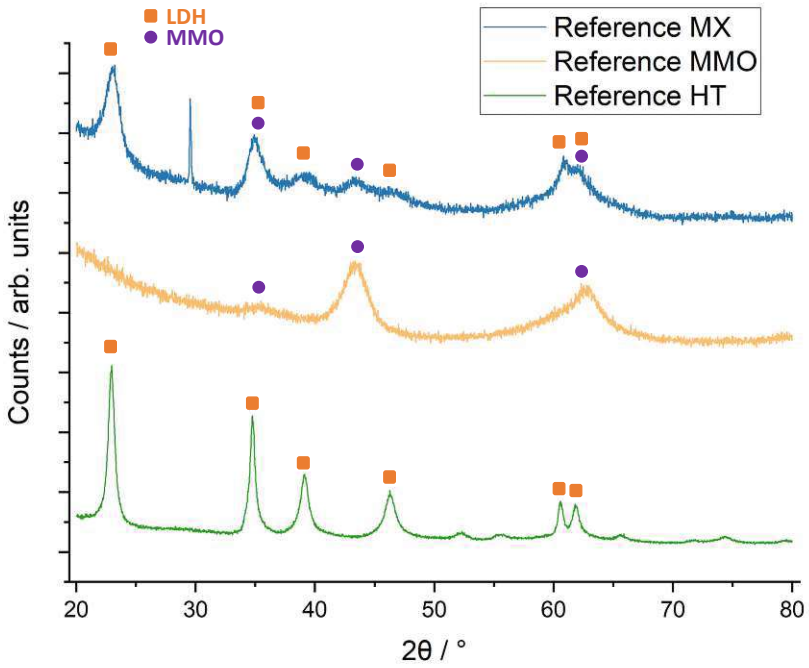

Figure 14: Diffractograms of reference Mg:Al material as HT, MMO and after rehydration for 20 min at RT. Reflections were assigned to LDH and MMO phases.

XPS measurements were performed to examine the surface composition of the material. In Figure 15 it can be seen that for samples with low Al content the surface ratio more or less corresponds to the nominal ratio while at higher Al contents more Al is on the surface than would be expected. This could be a hint that the preparation method does not lead to sufficient diffusion of Al through the sample. For the rehydrated Mg:Al 30:1 sample the ratios are correct once again, correlating with the appearing of $Mg(OH)_2$ in the bulk phase.

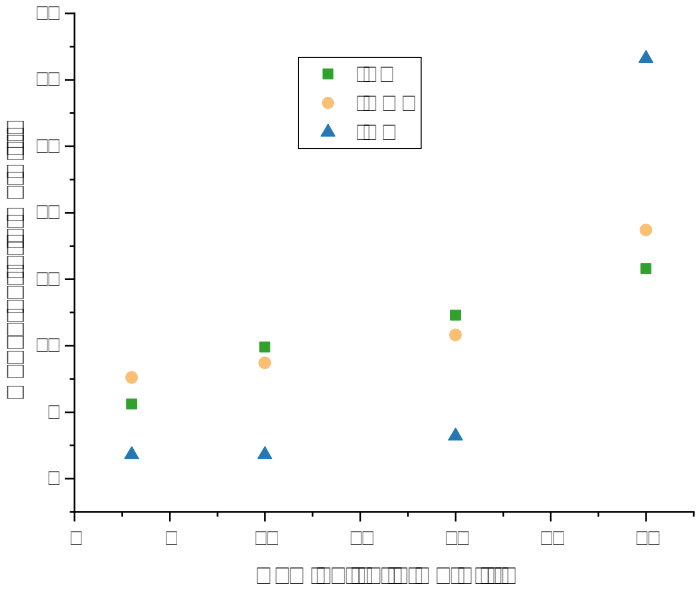

Figure 15: Theoretical ratio of Mg and Al in the examined samples and measured ratio of Mg and Al on the surface determined via XPS.

3.1.4 Copper-containing materials

Copper-containing oxides were synthesized as potential hydrogenation catalysts. As a result of the inclusion of copper, the materials show distinct color changes depending on its state (HT, MMO, reduced). With lower copper content the colors are less intense as can be seen in Figure 16.

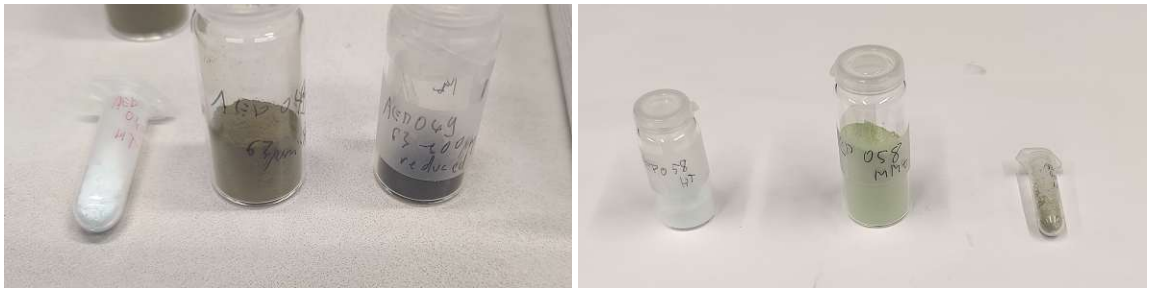

(a) (b)

Figure 16: Pictures of (a) 1:1:1 Cu:Mg:Al and (b) 0.2:1.8:1 Cu:Mg:Al. From left to right each: HT, MMO and reduced MMO.

The surface area was measured for the reduced material. It can be seen in Table 4 that the catalyst with high copper loading has lower surface area, while the material with less copper is in the range of pure Mg:Al MMO. This effect is also reported in literature [43], although it is even more pronounced there.

Table 4: BET surface area of reduced copper containing MMO catalysts.

Sample	BET surface area / $m^2\,g^{-1}$
1:1:1 Cu:Mg:Al	117
0.2:1.8:1 Cu:Mg:Al	247

Figure 17 shows the respective physisorption isotherms. According to the IUPAC definition [42] the shape of both can be classified as Type IV(a), suggesting a mesoporous material with pores $> 4\,nm$.

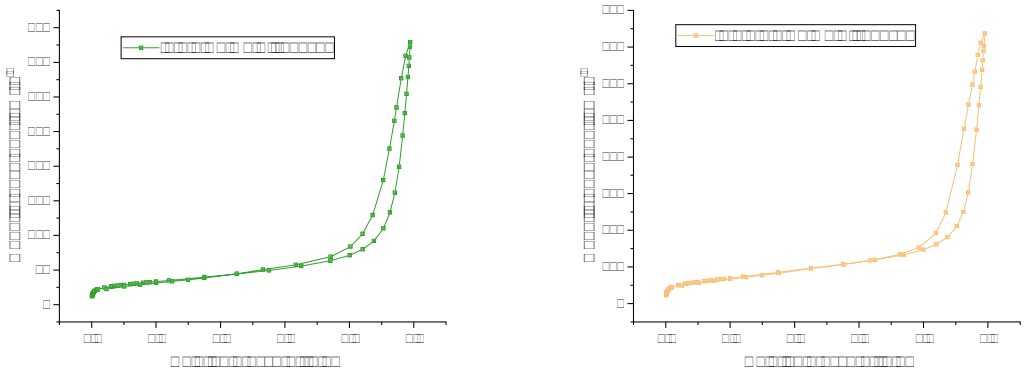

(a) (b)

Figure 17: Adsorption/desorption isotherms of (a) 1:1:1 Cu:Mg:Al MMO and (b) 0.2:1.8:1 Cu:Mg:Al MMO.

XRD measurements of the Cu-containing materials depicted in Figure 18 show normal HT and MMO formation with reflections that hint to Cu-containing phases visible in the 1:1:1 Cu:Mg:Al material, indicating successful incorporation of Cu in the structure.

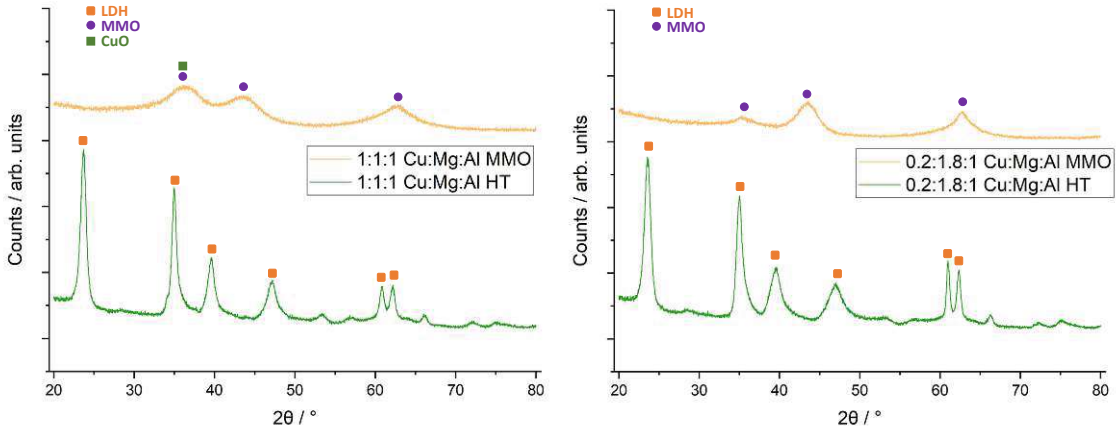

(a) (b)

Figure 18: Diffractograms of (a) 1:1:1 Cu:Mg:Al and (b) 0.2:1.8:1 Cu:Mg:Al as HT and MMO. Reflections belonging to HT, MMO and CuO were assigned.

When performing the reduction of the 1:1:1 Cu:Mg:Al in the gas flow reactor, after taking the material out of the reactor, it was observed that the powder will start taking back on the green color of the MMO. This reaction seems to spread in circles from random points of the material; only by quickly separating the color changing parts from the still-black parts the spreading of the reaction can be contained. The reaction is able to ignite weighing paper that comes into contact with the material.

Comparison of XRD data from black and green material (Figure 19) after the reduction step shows that both are MMO structures, the former with shifted peak heights compared to the 2:1 Mg:Al MMO and an extra reflection that both can be attributed to metallic Cu, while the latter seems to have reflections of CuO mixed into the pattern.

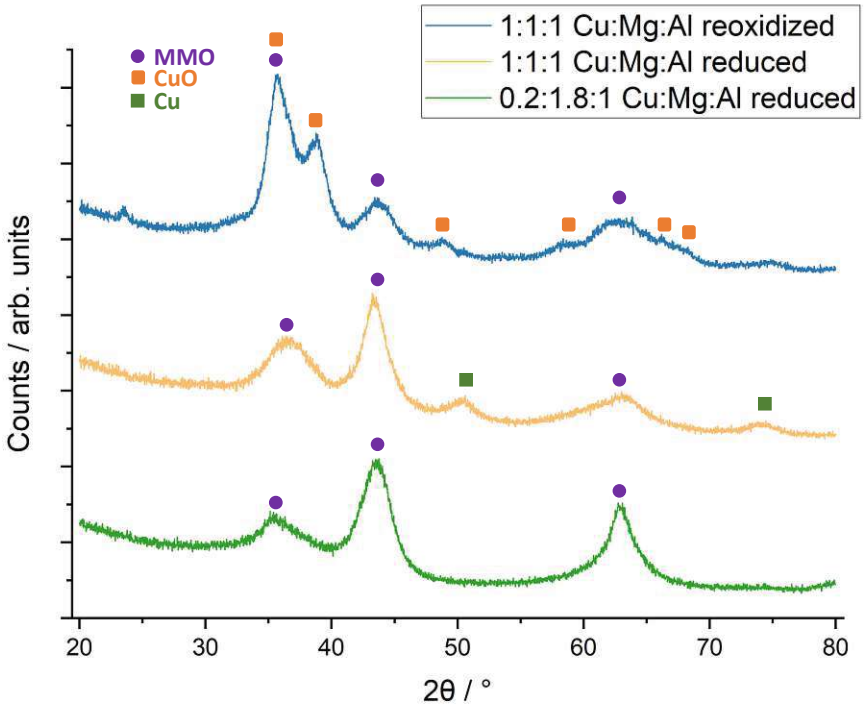

Figure 19: Diffractograms of 1:1:1 Cu:Mg:Al after reduction and after spontaneous reoxidation when exposed to air at RT as well as 0.2:1.8:1 Cu:Mg:Al after reduction. Reflections belonging to MMO, CuO and Cu phases are assigned in the diffractograms.

This points to the observed reaction being the reoxidation of Cu particles to CuO. A possible explanation for the spreading could be that this reoxidation is an exothermic reaction that provides enough heat for self-propagation upon other, previously unaffected parts of the material. [44]

It is not clear why some parts undergo the described reaction and others not. Influencing factors could be particle size, adsorbed hydrogen or passivation by trace amounts of oxygen that provide too little fuel for self-propagation of the reaction.

When performing the reduction while doing TPR measurements the reduced, black sample also gets in contact with air after removing the sample from the oven. The reoxidation reaction as described above was not observed in those cases. It was assumed that this is due to a less airtight setup leading to slower passivation of the copper particles on the surface.

The TPR results show only one peak for all MMO material as can be seen in Figure 20.

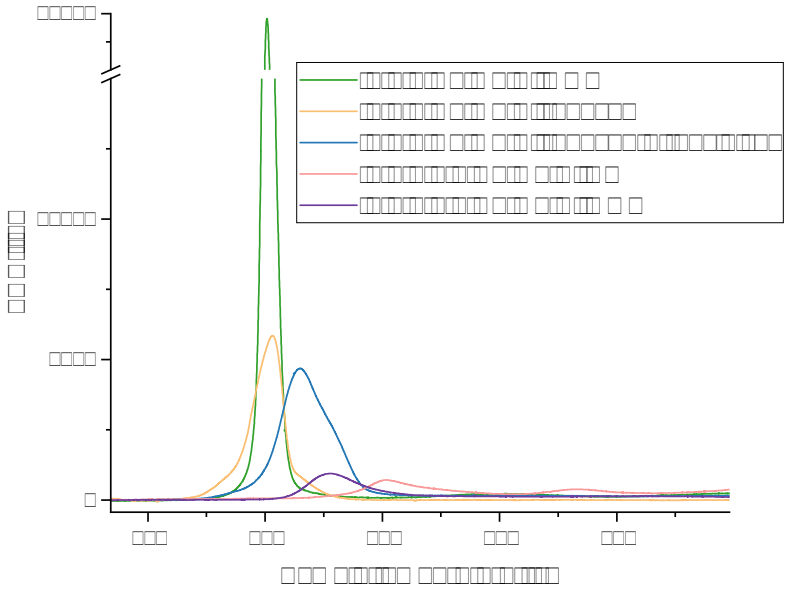

Figure 20: TPR results of 1:1:1 Cu:Mg:Al and 0.2:1.8:1 Cu:Mg:Al materials. For 1:1:1 Cu:Mg:Al reduced baseline correction was performed to correct for a high, curved background that was determined to be the result of inadequate equilibration time for the TCD.

The already reduced, visually black material has a small peak in the same temperature region as the MMO (200 °C), indicating that on a scale not visible to the human observer still some oxidation of the material happens, which however does not initiate a self-propagating reaction. This could be supportive of the theory of passivized Cu mentioned above. However, this also means that, whenever possible, a reductive pre-treatment of the catalyst should be performed to ensure maximum efficiency.

The reduction temperature of the 'mixed' material (black and green MMO after reduction) is shifted to higher temperatures of about 200 °C to 300 °C. Lower copper content leads also to a shifted peak with a maximum rate of reduction at about 250 °C.

TPR of HT material does not show a peak in the same region as for MMO catalysts, but instead two broad bands centered around 300 °C and 475 °C with a rising baseline at the end of the measurement. Therefore, another peak at over 600 °C can not be ruled out from this measurement. The different shape of signals compared to MMO material can be attributed to release of interlayer H_2O and CO_2.

For each sample a calibration was performed to establish a relationship between the TCD signal and the mass flow of H_2. This can then be used to convert to the total amount of H_2 used after integration of the peaks. The general equation for reduction of oxides is shown in Equation 1. [45]

$$M_xO_y + y\,H_2 \longrightarrow x\,M + y\,H_2O \tag{1}$$

This was used together with the known masses of the samples to relate the amount of H_2 used (Table 5) to the percentage of the material reduced as shown in Table 6. Additionally, the reduced amount of CuO was calculated, as it was assumed that this was the only species reduced under the used conditions. The TPR measurements of the HT material were excluded from quantitation, as due to the likely release of H_2O and CO_2 it was not possible to simply attribute a change in TCD signal to a reduction process.

Table 5: Quantitative results of TPR performed on Cu:Mg:Al catalysts (H_2 consumed per catalyst amount).

Sample	H_2 consumed / mmol g^{-1}
1:1:1 Cu:Mg:Al reduced	2.4
1:1:1 Cu:Mg:Al reduced + reoxidized	2.6
1:1:1 Cu:Mg:Al MMO	3.8
0.2:1.8:1 Cu:Mg:Al MMO	0.7

Table 6: Quantitative results of TPR performed on Cu:Mg:Al catalysts (percentage reduced).

Sample	Sample reduced / %	CuO reduced / %
1:1:1 Cu:Mg:Al reduced	12	41
1:1:1 Cu:Mg:Al reduced + reoxidized	13	45
1:1:1 Cu:Mg:Al MMO	18	64
0.2:1.8:1 Cu:Mg:Al MMO	2	39

Table 6 shows that up to half of the CuO gets reduced under the chosen conditions. Moreover, the material that has undergone a prereduction and visibly still had the black color of the reduced material, also was reduced further.

It can also be seen that the difference in amount of reduction between the prereduced samples and the MMO was only about 20 percentage points. However, it should also be noted that the calculations for the prereduced material have high uncertainties since the exact composition of the material before TPR cannot be known.

Therefore the quantitative data has to be interpreted very conservatively and the main conclusion drawn is that the presence of further reduction of the already reduced sample is another sign of reoxidation. Reasons for possibly incomplete reduction of the MMO under TPR conditions need further research to be elucidated.

The apparent reactivity of the catalyst together with evidence of formation of copper indicates a promising candidate for reduction reaction. The low point of reduction at below 250 °C will further facilitate hydrogenation experiments since the reduction of the catalyst then can be performed in-situ with the available flow reactor.

3.2 Spinel and magnesium oxide catalysts

As exemplary spinels $MgAl_2O_4$ and $CoAl_2O_4$ were successfully synthesized through thermal decomposition, MgO was prepared via precipitation by addition of base and subsequent calcination. In case of $MgAl_2O_4$ and MgO a white powder was obtained, while $CoAl_2O_4$ presented as a dark grey/black powder. Those findings are consistent with literature, as it was previously described that the color of $CoAl_2O_4$ depends on the temperature of calcination with the characteristical blue color only appearing when calcining at 550 °C or above. [46] The samples were characterized by XRD, N_2 physisorption and (in case of $MgAl_2O_4$) SEM.

XRD confirmed the formation of a spinel phase for both materials as seen in Figure 21 (a). In Figure 21 (b) the diffractograms of precipitated Mg before calcination (upper graph) and after calcination (lower graph) are shown. Before calcination the pattern is that of $Mg(OH)_2$, after calcination MgO has formed.

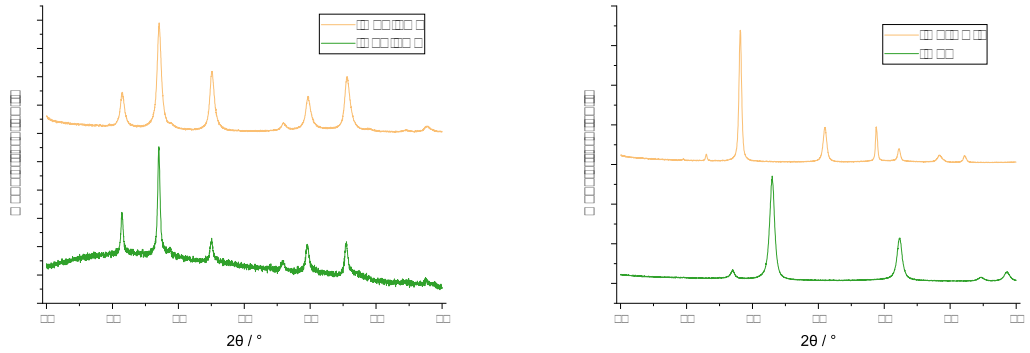

(a) (b)

Figure 21: Diffractograms of (a) Co:Al and Mg:Al spinel catalysts (1:2) prepared by thermal decomposition (b) $Mg(OH)_2$/MgO catalyst prepared by precipitation.

BET results are depicted in Table 7, showing that precipitated MgO has double as much surface area as calcined $MgAl_2O_4$. Both are still significantly lower than the surface area of the MMO catalysts.

Table 7: BET surface area of oxide catalysts.

Sample	BET surface area / $m^2\,g^{-1}$
$MgAl_2O_4$	61
MgO	135

Figure 22 shows the respective physisorption isotherms. According to the IUPAC definition [42] the shape of both can be classified as Type IV(a), suggesting a mesoporous material with pores > 4 nm.

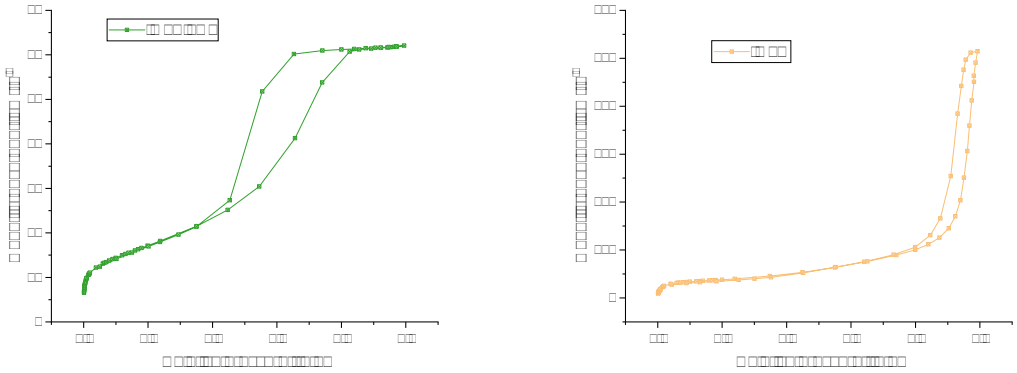

(a) (b)

Figure 22: Adsorption/desorption isotherms of (a) $MgAl_2O_4$ prepared by thermal decomposition (b) MgO prepared by precipitation.

The SEM images can be seen in Figure 31 (a) and show that the surface of $MgAl_2O_4$ consists of relatively large crystals with smaller structures grown onto it. While the surface is mostly smooth, upon closer examination some parts with rugged surface can be found as for example in Figure 23 (b).

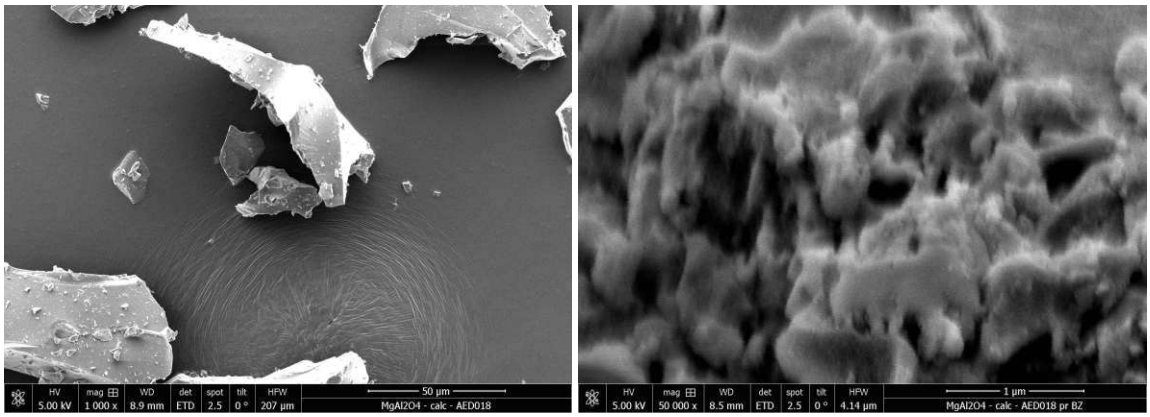

(a) (b)

Figure 23: Recorded SEM images of selected parts of $MgAl_2O_4$ spinel surface at (a) 1 000 x magnification. (b) 50 000 x magnification.

3.3 Aldol condensation

3.3.1 Reference reactions using NaOH

Before starting systematic catalytic tests of oxide materials, aldol condensations were performed at room temperature (about 23 °C) using NaOH as catalyst to get a reference for how long a reaction should take. As the reaction is performed in acetone, NaOH is used as a heterogeneous catalyst here.

In those reactions, it was noticed that the NaOH started agglomerating and taking on a light yellow color. Since sometimes also a second phase on the bottom of

the vial could be observed, it is speculated that this agglomeration is caused by formation of condensation water. One possible mechanism for this would be the solvation of NaOH by the condensation water, and by subsequent absorption of the water by material clogging happens due to the resulting precipitation of NaOH. Another possibility would be the adsorption of organic material (e.g. oligomers forming during the reaction) The reaction mixture itself became gradually darker, from clear to yellow, continuing to orange and finally turning dark brown.

After a reaction time of 1 h, complete conversion of benzaldehyde was found through GC analysis, resulting in a wide range of products with one peak dominating as seen in Figure 24. This main product could not be identified. Its retention time did not match that of benzylideneacetone, dba or benzylalcohol. Also, significant amounts of DAA and MES had formed.

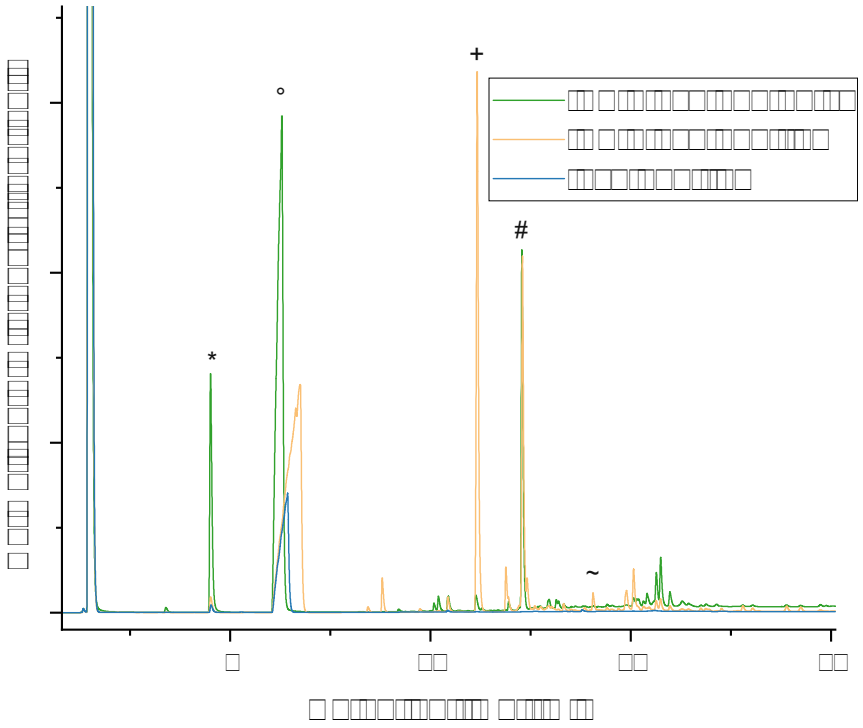

Figure 24: Chromatograms of preliminary tests using NaOH as catalysts at room temperature. Chromatograms were normalized to solvent peak to correct for variations in injection volume. Identified compounds are marked in the chromatograms: * MES ° DAA + unknown main product # BZcon ∼ dba.

During the flow reaction test with benzaldehyde at first the product stream was dark brown, then got a significantly lighter color. As main products DAA, benzylideneacetone and the unknown product also seen in the batch reaction tests were observed. The formation of MES was less than during batch tests.

After 1 h, the reaction was stopped because of leaking. It was assumed that this was caused by the agglomeration of Na_2CO_3 and/or NaOH leading to increased backpressure.

When doing the test with pure acetone, it was noticed that even with very short contact time (about 3 s) DAA was formed in notable quantities (see Figure 24), although the conversion to MES was much lower.

The preliminary tests gave valuable information for the conduction of the following tests with oxide materials. Reaction mixtures are expected to change color upon successful reaction. DAA, MES and condensation products of aldehyde and acetone are expected products. Cannizzaro reaction does not seem to be a relevant side reaction under the chosen conditions. Deposition of organic matter is an obstacle that can occur when performing aldol condensations in flow conditions which can lead to catalyst deactivation. For reactions using NaOH as catalyst also the formation of condensation water can be a relevant hindrance.

3.3.2 Comparison of catalysts in batch reactions

To ensure consistency between reactions, a batch reactor with highly defined conditions was used. Before starting experiments a pressure test (see chapter 7.4) was performed. The reactor was filled with 100 mL of acetone and heated to 150 °C. A maximum pressure of 6 bar was recorded, concluding that it was safe to operate the batch reactors in experiments using acetone that would not exceed 100 °C as the recorded pressure is lower than the reactor limits.

Batch reactions were performed to compare the catalytic activity of the synthesized oxide materials for aldol condensations and to decide which catalysts were to be used in flow conditions, since those experiments are more time-consuming.

Since the the quantitative GC method for aldol condensations was still under development at the first stage of the batch reactor experiments, mostly only qualitative observations can be made about the activity of spinel catalysts. Evaluation using the area-% of the respective peaks is used as an alternative quantifier to get an estimation for the conversion of BZ and the distribution of the products. In those cases, the relative peak areas of the identified compounds were assumed to be an acceptable estimation for the relative concentrations of the analytes.

Figure 25 shows that with increased temperature, the activity of the catalysts also increases. The difference in the activation energy for aldol reaction and dehydration could explain the marked jump in concentration for MES. [3]

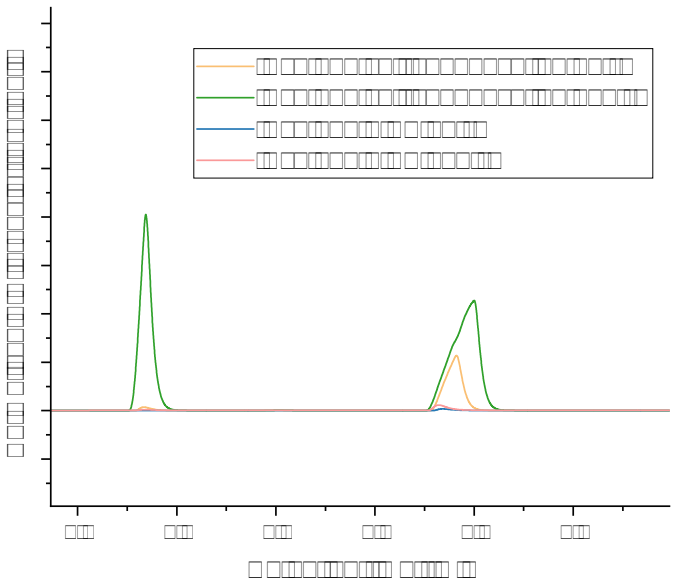

Figure 25: Section of chromatograms of acetone self condensations and aldol condensations of acetone and BZ performed in the batch reactor using $MgAl_2O_4$ as catalyst at different temperatures (4 h). Left peak (RT 3 min): MES, right peak (RT 5.9 min): DAA. Chromatograms were normalized to solvent peak to correct for variations in injection volume.

Table 8: Conversion of BZ calculated based on the area-% of BZ and the identified products for batch reactions (4 h) with $MgAl_2O_4$ as catalyst.

Temperature / °C	Conversion BZ / %
60	1
100	2

This is also supported by Table 8, although the relative difference is very low, as spinel catalysts in general showed low activity as can be seen in the comparison of different materials of Table 9 and Table 10. Overall, MgO and 2:1 Mg:Al MMO performed best, reaching conversions of 30 % to 40 %.

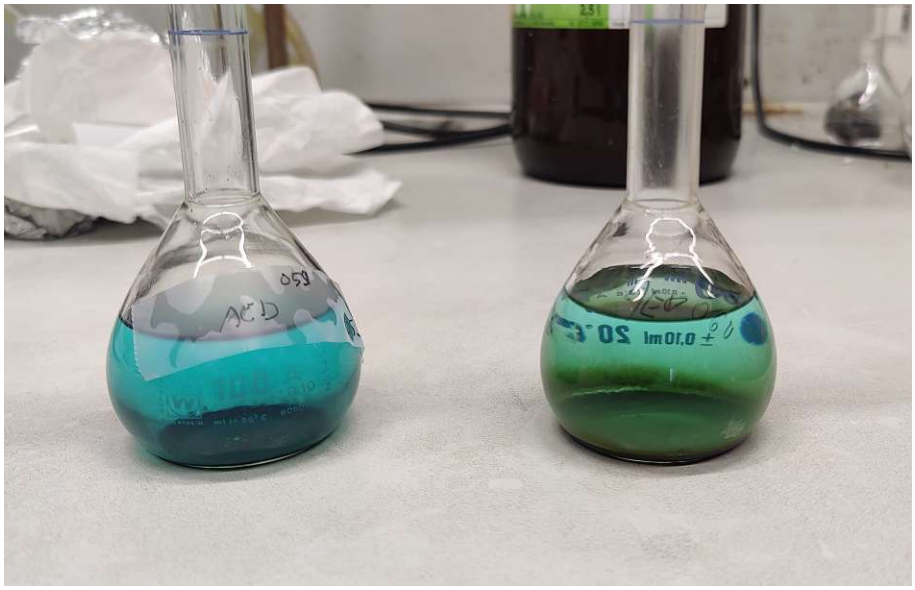

Figure 26: Reaction mixture after batch aldol condensation (50 °C, 4 h) using 1:1:1 Cu:Mg:Al in reduced form (left) and in MMO form (right) and letting the catalyst particles settle for 24 h.

Inclusion of Cu in the MMO structure reduced the activity considerably. However, it is notable that the difference between the conversion calculated via GC calibration and the conversion calculated using the area of the peaks differs by 10 to 20 percentage points for those reactions. This activity can be contrasted to findings of similar studies [47], where Cu supported on $MgAl_2O_4$ spinel had comparable conversion as unmodified $MgAl_2O_4$ and was successfully used both for aldol condensation of HMF (although at temperatures of 140 °C) and the subsequent hydrogenation of the products.

This disparity is possibly explained by the fact that another peak was seen in the chromatograms of the reactions catalyzed by Cu-containing material (see Figure 27), which could be another product that was not identified and therefore not accounted for in the area-% conversion. Furthermore, the reaction mixture after the reaction is discolored blue (see Figure 26), which could indicate leaching of Cu into the solution. Further studies need to be performed to confirm this assumption.

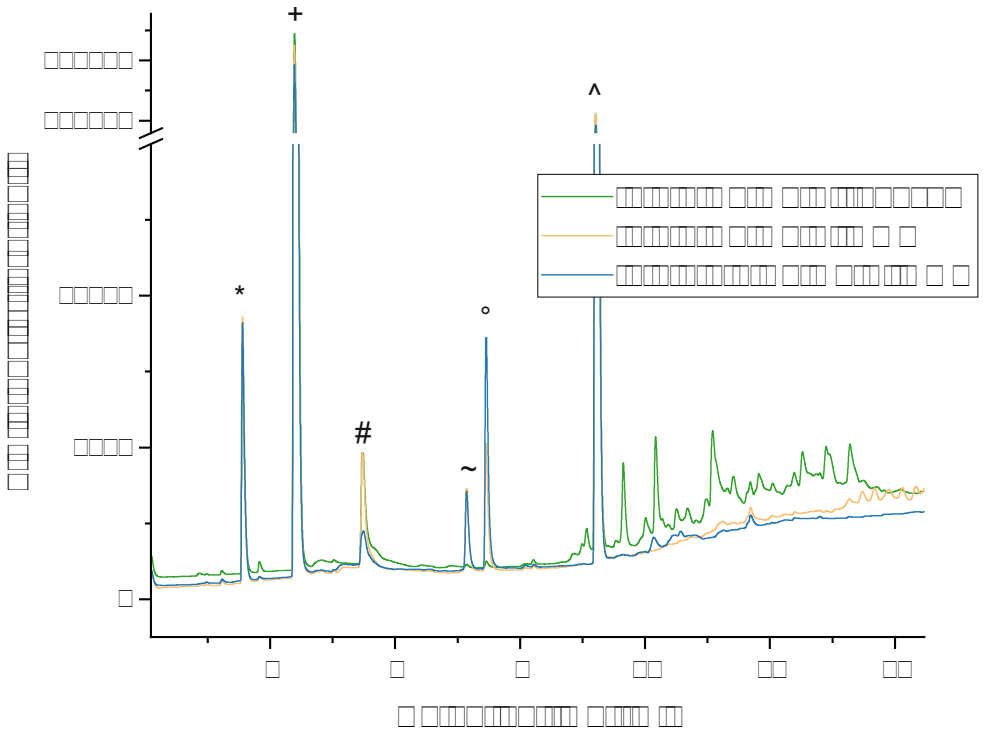

Figure 27: Chromatograms of batch reactions using different CuMMO materials as catalysts. Identified compounds are marked in the chromatograms: * DAA + BZ # unidentified peak ˜ BZcon ° unknown product, probably aldol ∧ internal standard.

Table 9: Results of batch aldol condensations between acetone and BZ using different catalysts (50 °C, 4 h). For the spinel catalysts no quantitative GC results are available as no method was established at the time of the experiment. Selectivities are calculated based on the area-% of the product peaks. BZcon also includes the unknown product as separation was not possible at the time of the batch reactions.

Catalyst	$MgAl_2O_4$	$CoAl_2O_4$	MgO
Area-% conversion / %	1	1	40
GC conversion / %	-	-	30
Selectivity Bzcon / %	78	82	92
Selectivity dba / %	22	18	8
M DAA / mol L^{-1}	-	-	0.074
M MES / mol L^{-1}	-	-	< LOD (0.004)

Table 10: Results of batch aldol condensations between acetone and BZ using different MMO catalysts (50 °C, 4 h). All (Cu:)Mg:Al materials were used in their freshly calcined MMO form. Selectivities are calculated based on the area-% of the product peaks. BZcon also includes the unknown product as separation was not possible at the time of the batch reactions.

Catalyst	2:1 Mg:Al	1:1:1 Cu:Mg:Al	0.2:1.8:1 Cu:Mg:Al
Area-% conversion / %	34	5	8
GC conversion / %	27	24	21
Selectivity Bzcon / %	94	87	95
Selectivity dba / %	6	13	5
M DAA / mol L^{-1}	0.043	< LOD (0.002)	< LOD (0.004)
M MES / mol L^{-1}	< LOD (0.003)	< LOD (-)	< LOD (-)

The deactivation of the 2:1 Mg:Al MMO catalyst was researched by taking samples at multiple timepoints during reactions. The samples were taken during the reaction without cooling down the solution. It was noted that while the distribution between mono- and double-condensation product stayed the same throughout the reaction, the conversion increased rapidly in the beginning of the reaction. That rate started dropping off starkly after as little as 0.5 h as Table 11 shows. Also, the catalyst was discolored yellow to brown after use. Those findings indicate some deactivation of the catalyst or reaching of an equilibrium which was then further examined by studying the reaction under flow conditions.

Table 11: Results of time-dependent batch aldol condensations at 50 °C using acetone and BZ with 2:1 Mg:Al MMO as catalyst. Conversion of BZ and selectivities calculated based on the area-% of BZ and the identified products. BZcon also includes the unknown product as separation was not possible at the time of the batch reaction.

Run	Time / h	Area-% conversion / %	Selectivity Bzcon / %	Selectivity dba / %
1	0.5	46	96	4
1	1	56	95	5
1	2	59	95	5
2	6	42	95	5
2	27	56	95	5

The reliability of the batch reactions was controlled by performing the aldol condensation with the same catalyst on different occasions. While the tests came very close to each other using the same batch of material, when changing to another batch it proved to achieve only about half of the conversion as Table 12 shows.

Table 12: Results of repeated batch aldol condensations using acetone and BZ with 2:1 Mg:Al MMO catalysts performed at 50 °C. The first three runs were performed with the same batch of material. *Sample was taken after 6 h (otherwise 4 h). No quantitative data is available for the first run. Selectivities are calculated based on the area-% of the product peaks. BZcon also includes the unknown product as separation was not possible at the time of the batch reaction.

Run	1*	2	3	4
Area-% conversion / %	42	35	34	15
GC conversion / %	-	22	27	18
Selectivity Bzcon / %	95	95	94	92
Selectivity dba / %	5	5	6	8
M DAA mol L^{-1}	-	0.042	0.043	0.019
M MES mol L^{-1}	-	< LOD (-)	< LOD (0.003)	< LOD (0.003)

3.3.3 Flow reactions

2:1 Mg:Al MMO was selected as the most promising candidate for aldol reaction catalysis. Flow reactions were performed to gather information about catalytic activity, selectivity and stability of the catalyst in continuous processes.

Repeatedly, problems with increase of pressure leading to leakage of the system occurred as a result of clogging of the PTFE filter installed directly upstream of the backpressure module. Black debris was identified as the cause of the blockage, which was assumed to stem from the rubber gaskets of the quick-connects. Chemical degradation through acetone was speculated to be the reason and as a consequence the quick-connects were removed from the system, after which the problem did not occur again. The in-line filter installed in the system after the CatCart and before the backpressure module (0.5 µm) was apparently insufficient to retain the debris. This highlights the importance of using chemically compatible parts for the set-up when using acetone as a solvent.

When performing flow reactions with a feed of BZ/acetone, the concentration of BZ will steadily increase until total deactivation of the catalyst as seen in Figure 28 (a). However, the product formation does not follow the same pattern. Instead, the amount of product will increase, reach a maximum and then decrease until deactivation. No steady-state equilibrium between BZ and BZcon was observed. A possible explanation could be the combination of diffusion pattern (little BZ and little BZcon at first) and deactivation of the catalyst (steady increase in BZ).

Figure 28 (b) shows that while there are considerable amounts of DAA formed, especially before BZ is introduced, very little is further converted to MES (< 5 %). The highest measured concentration of DAA (0.7 mmol mL^{-1}) converts to about 10.5 % (w/w), which corresponds to the expected equilibrium concentration of the reaction found to be between 9.1 % and 12.1 % at RT. [48]

Furthermore, it is visible that (in-situ) rehydration of the MMO increases the activity of the catalyst regarding both the aldol condensation between BZ and acetone as well as for the self-condensation of acetone.

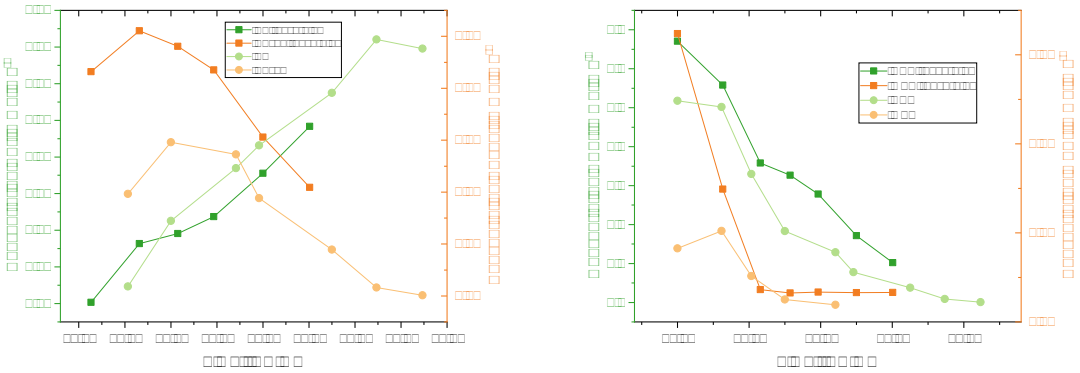

(a) (b)

Figure 28: Comparison of catalytic activity during selected flow reactions between 2:1 Mg:Al MMO and rehydrated 2:1 Mg:Al MMO. (a) Concentrations of BZ and BZcon. (b) Concentrations of DAA and MES.

That diffusion is relevant for the system, becomes apparent when looking at Figure 29 (a). Depending on the reaction, it takes up to over 4 h for the sum of concentrations of the starting material BZ and the main product BZcon to become constant. For the reaction using rehydrated MMO as the catalyst this equilibration time is significantly lower. This is probably a result of removing the quick-connects from the setup (see above) and thereby reducing its dead volume.

Using those results, a plot of the conversion of BZ and yield BZcon was created in Figure 29 (c). The measured concentrations of BZ and BZcon were plotted over time and divided by their combined concentration to try to minimize the influence of longitudinal diffusion in the reactor on the results.

It is also possible to plot the conversion and yield using the theoretical maximum possible conversion calculated with the initial masses weighed when preparing the feed. This has the advantage that other effects that can lead to lower conversions like other products than BZcon or loss of material on the column are also taken into account. Here it does not make sense to use the very first datapoint, as the effect of diffusion is probably high. Therefore, again looking at Figure 29 (a), the first datapoint is chosen where the plateau has already been reached.

Using this method, maximum BZ conversion would be about 75 % and maximum BZcon yield about 50 % for the rehydrated MMO and about 50 % and 30 % respectively for the non-rehydrated MMO which can be seen in Figure 29 (b). However, it has to be stated that these graphs is primarily intended for better visualization of the results and qualitative comparison between the two catalysts and not exact quantification of the yields.

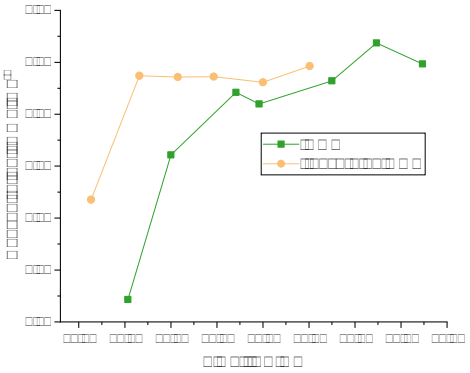

(a)

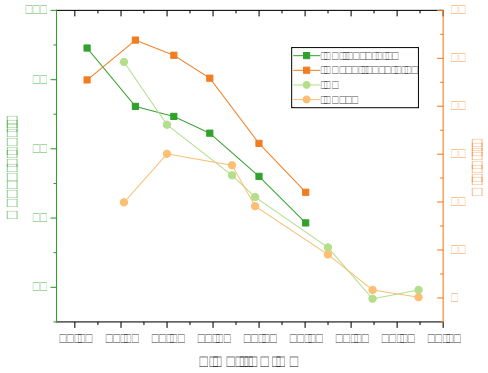

(b)

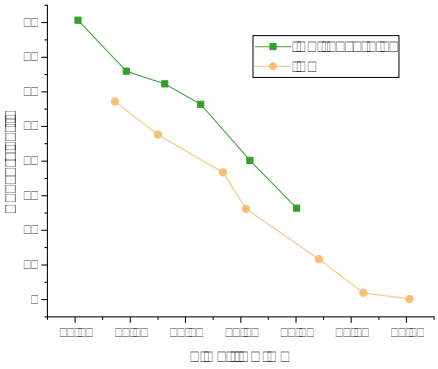

(c)

Figure 29: (a) Sum of BZ and BZcon during flow reactions with 2:1 Mg:Al MMO and rehydrated 2:1 Mg:Al MMO. (b) Estimated conversion of BZ and yield for BZcon for flow reactions with 2:1 Mg:Al MMO and rehydrated 2:1 Mg:Al MMO. (c) Estimated conversion based on sum of BZ and BZcon.

Selectivity of the catalyst was monitored through estimation of the distribution using the area% of the GC peaks of the three identified main products: BZcon, dba and an unknown product. To adjust for variability between injections, the percentages were normalized to the internal standard.

As shown in Figure 30, over time of the reaction the relative amount of BZcon produced decreases over time, while the amount of the unknown product increases.

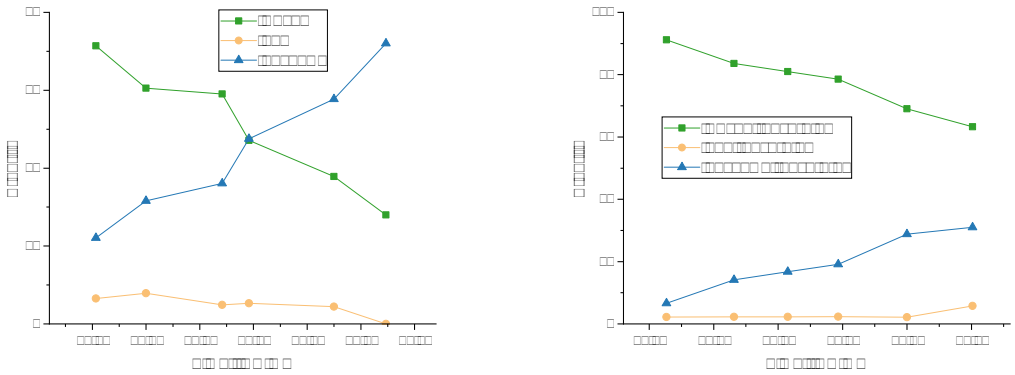

(a) (b)

Figure 30: Product distribution in flow aldol condensation of BZ and acetone for (a) 2:1 Mg:Al MMO (b) rehydrated 2:1 Mg:Al MMO.

This leads to the assumption that the unknown product is the respective aldol product 1-hydroxy-1-phenyl-3-butanone and that, with proceeding deactivation of the catalyst, it is losing its ability to completely convert BZ to BZcon. This is also supported by the fact that the selectivity for BZcon is generally higher for the overall more active rehydrated MMO. The trend of rehydrated MMO leading to less byproducts also fits to the estimated yields in Figure 29. Dba is generally only produced in low quantities.

MMO catalysts have proved to effectively convert acetone to DAA and BZ to benzylideneacetone in flow reactions at room temperature. In-situ rehydration of the catalyst can improve its activity. However, quick deactivation of the catalyst proves to be a challenge.

3.3.4 Distribution of products

The main product of the acetone self condensation was DAA, only in some batch reactions significant formation of MES was seen. During batch aldol condensations it was observed that when performing the reaction with acetone and BZ, the formation of DAA was almost completely suppressed in most of the experiments (see Figure 25). Similar effects have been reported in literature when comparing self-condensation of acetone and cross-condensation with an aldehyde. [47]
A possible explanation could be that BZ binds stronger to the surface and therefore blocks catalytic sites for acetone. Further mechanistic studies would be needed to explain this phenomenon. This suppressive effect was not seen in flow reactions.

In section 3.3.3 an unknown product is mentioned. This refers to a second peak eluting closely after BZcon. It is assumed that this is the respective not dehydrated aldol product 1-hydroxy-1-phenyl-3-butanone. For most of the batch reactions the GC method was not yet developed enough to resolve BZcon and the unknown peak, therefore those products are reported together in section 3.3.2.

3.3.5 Deactivation of catalysts

Deactivation of the MMO catalysts was observed in various experiments as already discussed in chapter 3.3.3. In Figure 28 it can be seen that after a stable concentration of DAA when only flowing acetone is observed, the concentration starts to drop immediately after BZ is also reaching the catalyst (when compared, the onset of drop in DAA concentration in Figure 28 (b) with onset of BZ/BZcon in Figure 28 (a) happen at the same time).

It was not distinguishable if this happens because of competition between acetone and BZ for catalytic sites or because of deactivation of the catalyst. To see if that change was reversible, a experiment was conducted where acetone was flowed for 2 d, then BZ overnight until deactivation, then aceton again for 2 d.

Table 13: Concentration of DAA over course of reaction switching feed between acetone and acetone/BZ and back.

Reaction time / d	Feed	Concentration DAA / mmol mL^{-1}
1	Acetone	0.592
2	Acetone	0.574
2	Acetone/BZ	0.295
3	Acetone/BZ	< LOQ (0.010)
4	Acetone/BZ	< LOD (0.009)
5	Acetone	< LOD (0.009)

The concentration of DAA did not rise again after flowing acetone again as Table 13 shows. From that observation it can be concluded that deactivation induced by BZ can not be reverted by flowing acetone.

At least for $MgAl_2O_4$ catalysts no overall change in morphology could be noticed that would explain catalyst deactivation as seen in Figure 31. Figure 32 shows 2:1 Mg:Al MMO that was recovered after use in flow reactions. After standard flow reactions with BZ and acetone or only acetone the previously white MMO was only slightly yellow discolored, while the rehydrated MMO had a darker color. It is speculated that this connects to the higher activity of the rehydrated MMO catalyst established in section 3.3.3.

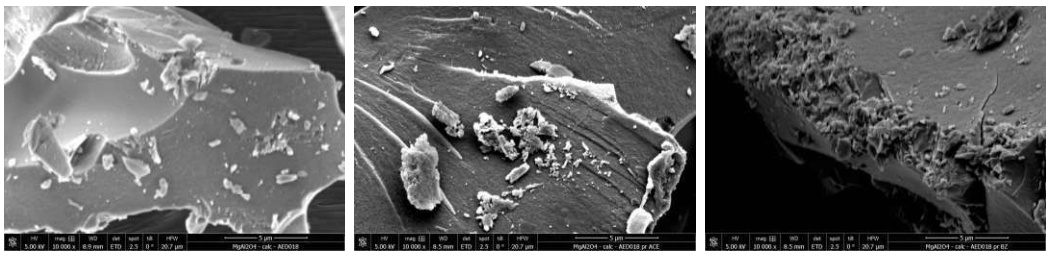

(a) (b) (c)

Figure 31: Recorded SEM images of $MgAl_2O_4$ spinel at 10 000 x magnification. (a) Before reaction. (b) After reaction with acetone. (c) After reaction with benzaldehyde.

During one reaction the O_2 flow was accidentally not cut off after the pre-treatment until 2 h after start of the acetone flow. As a result, the catalyst was rapidly deactivated and very strongly discolored after recovery as seen in Figure 32 (d). This correlation of dark color and fast deactivation strengthens the theory that organic matter built-up plays a role in the deactivation of the catalyst.

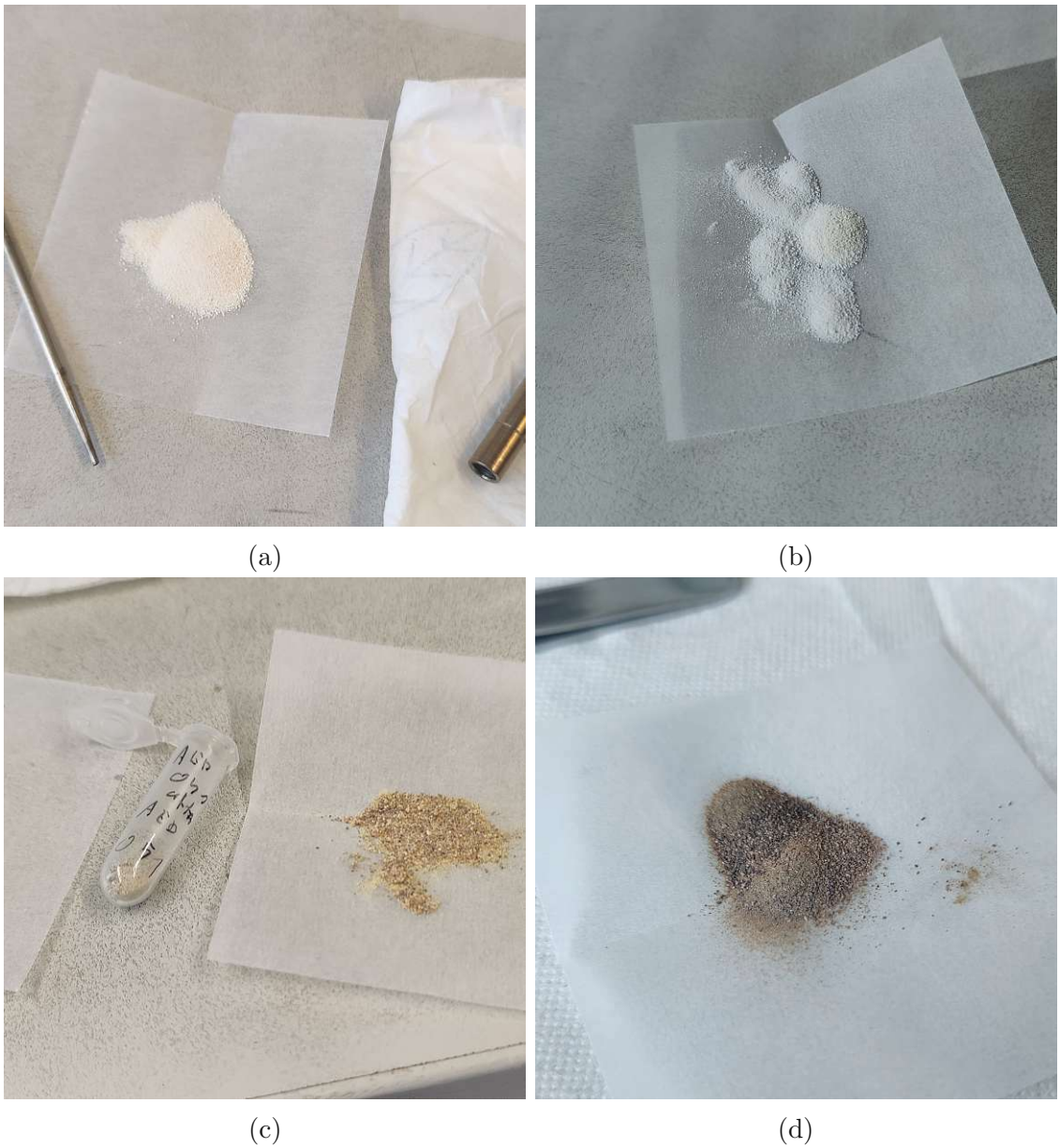

(a) (b)

(c) (d)

Figure 32: Pictures of 2:1 Mg:Al MMO after flow reactions. (a) After reaction with acetone. (b) After reaction with BZ and acetone. (c) Rehydrated MMO after reaction with BZ and acetone. (d) After reaction with acetone and O_2 flow.

Light brown MMO after a flow reaction with BZ was calcined at 450 °C. After calcination a white solid was obtained and a mass loss of 14 % was recorded. However, when using it for another flow reaction it did not achieve the same activity as before (highest recorded DAA concentration after 24 h on first run 0.47 mmol mL^{-1},

on second run 0.03 mmol mL^{-1}). This supports the theory that the discoloration is a result of organic matter deposition, but also indicates that either another mechanism of deactivation is also reason for deactivation or that the organic deposit can not sufficiently be removed by calcination at 450 °C.

3.4 Hydrogenation reactions

Previously reduced 1:1:1 Cu:Mg:Al was tested for flow hydrogenation at temperatures from 150 °C to 250 °C using BZcon in iPrOH as feed. At all temperatures complete conversion was achieved. As Figure 33 shows, at 150 °C selective hydrogenation to 4-phenyl-2-butanol can be achieved (see Figure 33), while with increasing temperature a wider array of products is obtained.

It has to be noted that because the reaction was performed at pressures of 20 bar due to a misjudgment of the vapor pressure of iPrOH at higher temperatures, it is possible that the reactions above 190 °C were performed inadvertently with iPrOH in the gas phase. This is however not certain, as the pressure inside the reactor was not measured. It can just be stated that the pressure measured at the HPLC pump was between 30 bar and 45 bar throughout the reaction while the backpressure module recorded pressures of about 20 bar. Therefore the pressure conditions throughout the reactor as well as before or after the reaction are not well defined and may vary.

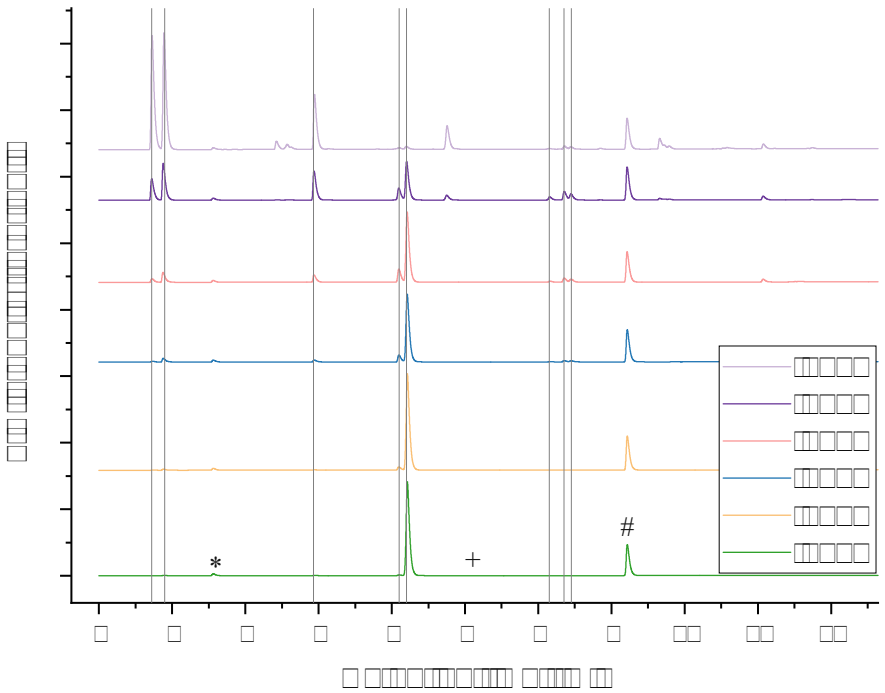

Figure 33: Chromatograms of flow hydrogenation of BZcon. Samples drawn at different reaction temperatures. * DAA from the acetone used for sample preparation + starting material # internal standard.

GC-MS analysis was performed on the sample taken at 230 °C and possible structures were proposed that are summarized in Table 14. The first 5 structures corresponds to the first 5 visible products in Figure 33, indicating that at higher temperatures a higher degree of C−C bond cleavage happens. The last three products seem rather counterintuitive, but could be a possible side effect of harsher reaction conditions, iPrOH being in the gas phase and direct contact of liquid benzylideneacetone with the reduction catalyst.

Table 14: Proposed identities of the main products based on GC-MS analysis and estimated distribution based on the area% of the peaks.

Retention time / min	Area / %	Proposed identity
2.7	12.3	Methyl isobutyl ketone
2.9	20.5	4-Methyl-2-pentanol
4.9	14.9	Butylbenzene
6.1	7.9	3-Phenyl-2-butanone
6.2	20.0	4-Phenyl-2-butanol
8.2	4.3	Heptylbenzene
8.4	6.8	Benzenepentanol
8.5	4.9	(2,4-Dimethylcyclopentyl)-benzene

Another experiment was performed to investigate reaction temperatures from 50 °C to 150 °C. Following the TPR results of Figure 20, the reduction was performed through the in-situ pre-treatment. As examples, chromatograms from the reaction performed at 50 °C and 130 °C as well as the results from the analysis of the feed are depicted in Figure 34, showing again complete and selective conversion to 4-phenyl-2-butanol.

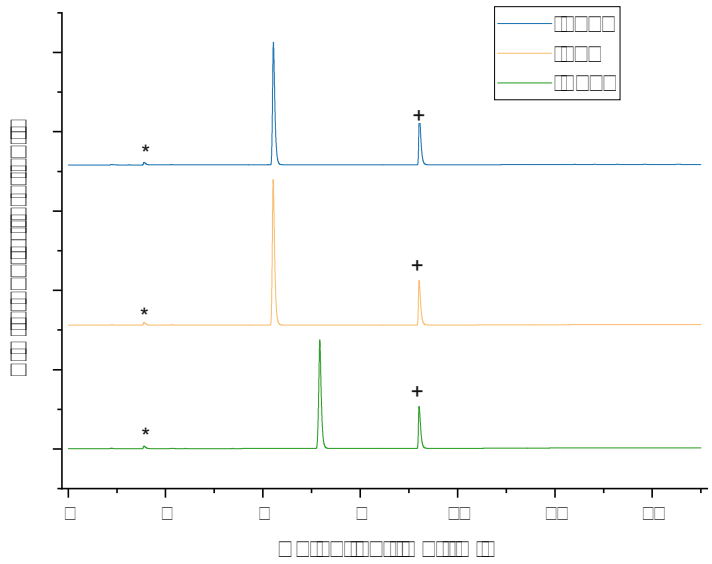

Figure 34: Chromatograms of flow hydrogenation of BZcon. Samples drawn at different reaction temperatures and the feed. In-situ reduced 1:1:1 Cu:Mg:Al MMO was used as catalyst. * DAA from the acetone used for sample preparation + internal standard.

A detailed look into the peak areas of the first reaction with prereduced catalyst is depicted in Figure 35, showing the development of the relative intensities of the peaks.

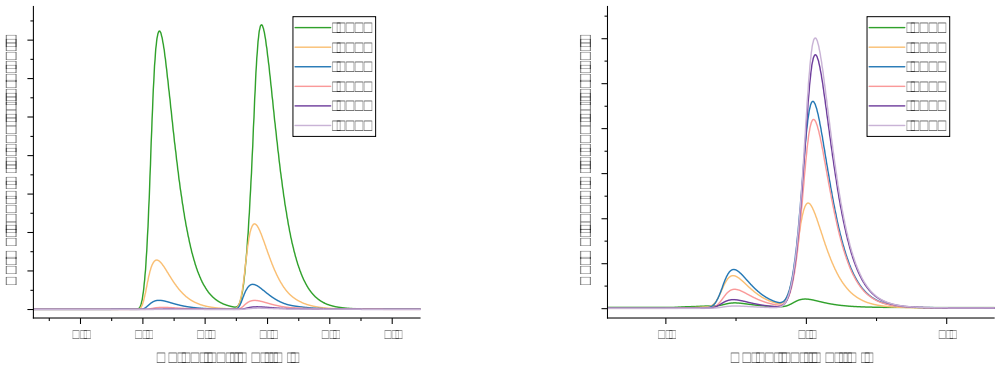

(a) (b)

Figure 35: Selected peaks in chromatograms of samples of flow hydrogenation of BZcon drawn at different reaction temperatures overlayed. (a) 4-Methylpentan-2-one and 4-methyl-2-pentanol (b) 3-Phenyl-2-butanone and 4-phenyl-2-butanol. Chromatograms were normalized to peak of internal standard to correct for variations in injection volume.

When performing the same reaction using furfurylideneacetone in iPrOH as feed, at

lower temperatures, the starting material was converted to one other product as can be seen in Figure 36. This process was not totally selective as was the case when using BZcon as feed with some other small peaks also appearing. This could indicate that the oxygen of the furfural ring leads to a more complex binding situation with the catalyst.

When exceeding the 190 °C again more extensive breakdown of the starting material starts to take place. At RT the catalyst did not show activity. However, when taking a sample of flowing just iPrOH one additional unexplained peak was noted that was not seen in other reactions at similar temperature.

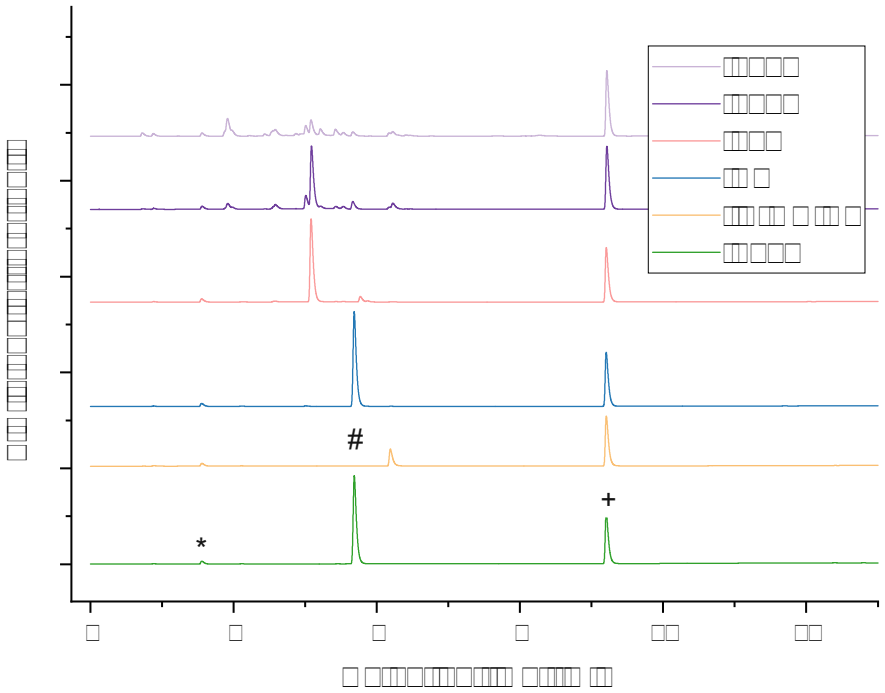

Figure 36: Chromatograms of flow hydrogenation of Fcon. Samples drawn at different reaction temperatures and the feed. In-situ reduced 1:1:1 Cu:Mg:Al MMO was used as catalyst. * DAA from the acetone used for sample preparation # Fcon + internal standard is visible at 9 min.

It was also noted when taken the sample at 250 °C, that the liquid was much less viscous than before. This fits the observation made that at this temperature there are significant changes in the whole reaction mixture.

To prepare for stability testing of the catalyst it was necessary to find reaction conditions under which the catalyst activity was lowered enough to operate in conditions where full conversion of the starting material is not reached. One possibility was explored through reduction of the Cu-loading by performing the flow hydrogenation using the 0.2:1.8:1 Cu:Mg:Al catalyst.

The resulting chromatograms are shown in Figure 37. Compared to previous tests with higher Cu-loading the catalyst shows less activity, with total conversion of the starting material only achieved at 150 °C. Further, it is visible that there are two main products whose relative concentration changes with temperature. The right one is the hydrogenation product 4-phenyl-2-butanol (identified by retention time) observed in the previous reactions. The left one then is probably one of the intermediates, with either only the double bond or only the carbonyl reduced. As with higher temperature the products go more towards 4-phenyl-2-butanol indicates that the reduction of the two sites each needs different conditions as was already expected by literature (see chapter 3.4). GC-MS measurements will be needed to gain more insight into the reduction mechanism.

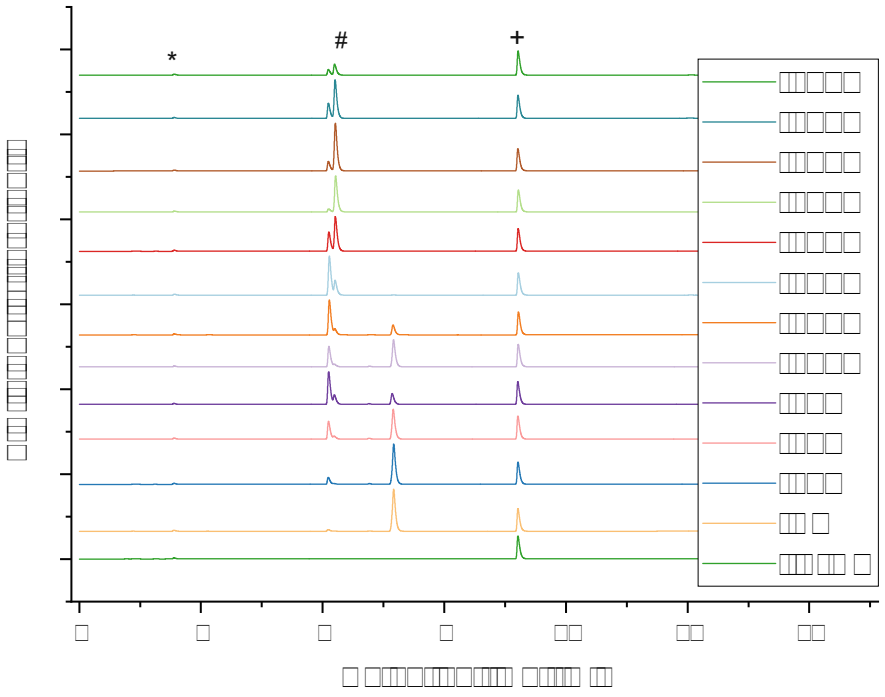

Figure 37: Chromatograms of flow hydrogenation of BZcon. Samples drawn at different reaction temperatures and the feed. In-situ reduced 0.2:1.8:1 Cu:Mg:Al MMO was used as catalyst. * DAA from the acetone used for sample preparation # 4-phenyl-2-butanol + internal standard.

When plotting the concentration of the starting material against the reaction temperature (Figure 38), a rise in concentration can be noticed. Time-wise, this correlates to an overnight part of the reaction and therefore prolonged reaction at 110 °C for about 18 h. This was interpreted as loss of catalyst activity over time and hints to limited stability under the chosen reaction conditions. Long-run studies will have to follow for exploring stability and kinetics of this catalyst class.

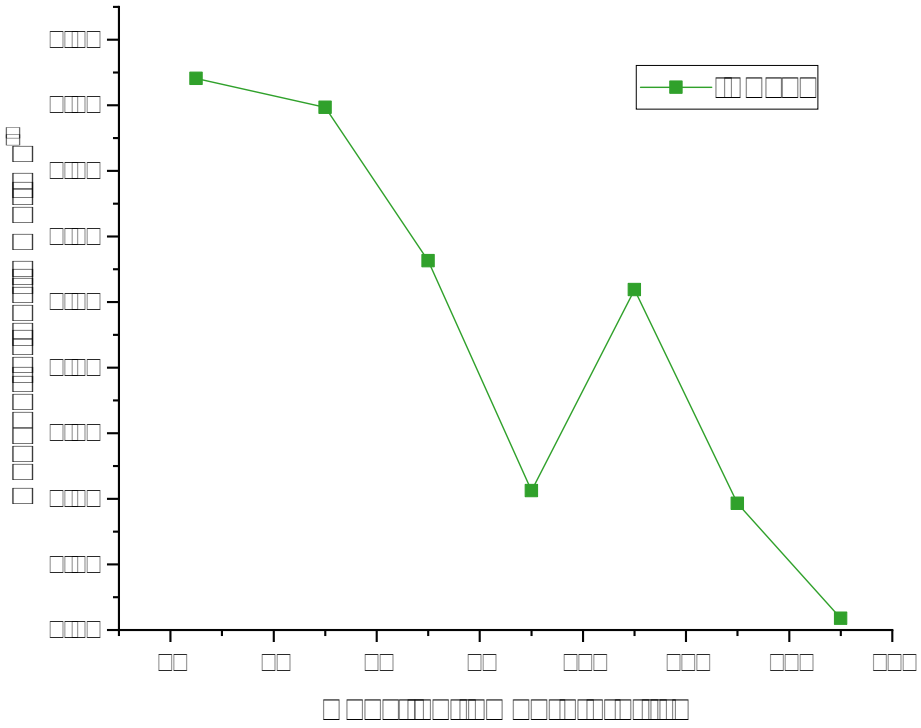

Figure 38: Concentration of BZcon against the reaction temperature during the hydrogenation reaction using in-situ reduced 0.2:1.8:1 Cu:Mg:Al MMO as catalyst.

4 Summary

MMO, MgO and spinel catalysts were successfully synthesized via coprecipitation and calcination methods and characterized using XRD, SEM and BET surface area measurements. It was established that by coprecipitation catalysts of higher surface area and more complex surface morphology can be made. Cu-containing mixed metal oxide catalysts were also synthesized and additionally investigated by TPR, showing low temperatures of reduction (200 °C to 300 °C) to yield supported metallic copper.

By performing aldol condensations in batch using a model system of acetone and BZ, 2:1 Mg:Al MMO was selected as the most promising candidate for flow reactions. MgO achieved comparable results, while spinels and Cu-MMOs were found to be comparatively inactive.

It was determined that MMO successfully converts BZ to benzylideneacetone, but suffers from fast deactivation (< 24 h). In-situ rehydration was found to increase catalytic activity, but not catalyst lifetime.

Cu-containing MMO were successfully used for the hydrogenation of benzylideneacetone in flow conditions with H_2, selectively yielding 4-phenyl-2-butanol at 50 °C. Furfurylideneacetone was also hydrogenated under those conditions, however, with minor byproducts. At higher temperatures hydrogenation goes further to yield more different products. It was asserted that the necessary reductive pre-treatment can be performed in-situ using a flow reactor yielding equivalent results as prereduction and pre-treatment.

GC-FID methods for quantifying the main products of the aldol condensation between acetone and BZ were developed. Dba and F2con were synthesized to be used for future reactions.

5 Outlook

While the work at hand established many basic observations of the properties of hydrotalcite derived materials in catalysis of aldol condensations and hydrogenations, more detailed studies will have to succeed to follow up on those discoveries.

One problem raised is the deactivation of MMO catalysts, and while it was speculated that organic matter deposition is responsible, experiments still have to be done to confirm this while also considering other possible causes. Long run flow studies with only acetone still have to be performed to see if the catalyst also deactivates under those conditions.

Mechanistic studies of the deactivation would be interesting to advance our understanding of heterogeneous catalysts. In particular, the cause for the suppression of DAA formation in batch reactions with BZ/acetone and the slow shift in products from benzylideneacetone to the presumed aldol during the deactivation would be possible starting points. Further investigations in the reaction mechanisms could also help to explain the different behavior of furfural-derived material compared to the BZ model system in hydrogenation reactions.

The next step towards environmentally friendly chemistry would be switching to bioderived aldehydes such as furfural or HMF as starting materials for aldol condensations. In preparation for further hydrogenation studies, dba and F2con were synthesized for use as possible starting materials. Performing the reaction directly with the products from the flow aldol condensations could be also desirable to streamline the process.

Optimization of copper loading, pressure, temperature and flow for the hydrogenation reactions to reach milder conditions is subject of currently ongoing investigations. Also, deactivation and stability of this catalyst class will be needed to be examined closer.

Last but not least, it will be necessary to examine the whole process and compare it to current industry standards to identify and establish cost and performance benchmarks for its viability.

6 Experimental

6.1 Data analysis

Basic data analysis was performed in Microsoft Excel 16.0. For data analysis of larger data sets and plotting OriginPro 2023b was utilized. Primary processing of GC data was done by LabSolutions Version 5.92, further processing of GC reports was done through Python 3.9. For identification of phases in recorded diffractrograms HighScore Plus 5.2 was used. Analysis of NMR spectra was performed using MestReNova 12.0.4-22023. Automatic analysis of BET surface measurement was performed by the ASAP 2020 V4.00 software. Reaction schemes were drawn with ChemDoodle 11.8.0. Annotations of figures were made in GIMP 2.10.32 and PowerPoint Version 2108. XPS data evaluation was carried out with CasaXPS software.

6.2 Chemicals

Table 15: Chemicals used with their origin and purity.

Chemical	Supplier	Purity
Acetone	Merck Millipore	for analysis
$Al(NO_3)_3 \cdot 9\,H_2O$	Riedel de Haën/Sigma Aldrich	98 %
Benzylideneacetone	Thermo Scientific	98 %
Benzophenone	Merck-Schuchardt	99 %
Biphenyl	Fluka Chemika	98 %
BZ	Sigma Aldrich	for synthesis
$Co(NO_3)_2 \cdot 6\,H_2O$	Sigma Aldrich	98 %
$Cu(NO_3)_2 \cdot 3\,H_2O$	Merck	for analysis
DAA	TCI	-
EtOH	Australco	96 % (1 % petroleum ether)
Fcon	Thermo Scientific	98 %
Furfural	Sigma Aldrich	for synthesis
Hydroquinone	Chemo-Droga GmbH	99.5 %
iPrOH	VWR	biotechnology grade
MES	TU intern	-
$Mg(NO_3)_2 \cdot 6\,H_2O$	Merck	99 %
Na_2CO_3 anhydrous	Merck	for analysis
NaOH	Thermo Scientific	for analysis
Cinnamonic acid	Merck-Schuchardt	99 %

6.3 Instrumentation

The **batch reactor** set-up was composed of a PTFE gasketed autoclave reactor equipped with an internal thermocouple and a PTFE liner (300 mL Series 4760 Pressure Vessel, Parr Instrument Company), a self-manufactured internal PTFE cap.

BET surface area analysis was performed using a Micromeritics ASAP 2020, using N_2 as adsorptive. A degassing step under high vacuum (< 17 mbar) was performed before the analyis. 0.1 g of material were used for the analysis. As all analyzed materials had appropriate isotherm shapes, for calculation of BET surface area 6 datapoints on the isotherm plot in the linear region between a relative pressure of 0.05-0.3 p/p° were taken.

For **centrifugation** a Sigma 2-16P Table centrifuge was used.

Flow reactions were done using a ThalesNano Phoenix system, consisting of the main oven, a control module, a gas module, a pressure module and a HPLC pump (model Knauer Atura P4.1S). The connections were built out of Swagelok parts, while the reactor parts were provided by ThalesNano. The reactor consisted of the CatCart as well as O-rings, filter and rubber fitting for closing the reactor. The CatCart was a 7 cm long steel plug flow reactor with 8 mm outer diameter and 4 mm inner diameter. For closing the CatCart a Gechter lever press was used.

GC-FID measurements were performed with a Shimadzu GC-2014 equipped with an autosampler of the model AOC-20i and an HP-5 column (crosslinked 5% PH ME silicone, length 30 m, inner diameter 0.32 mm, film thickness 0.25 µm). 1 µL of sample was injected with a split ratio of 16.8. He was used as carrier gas with a flow of 2.93 mL min^{-1}.

GC-MS measurements and database identification of analytes were performed by the research group of Ao.Univ.Prof. Dr.techn. Egon Erwin Rosenberg at the Institute of Chemical Technologies and Analytics, TU Wien.

^{1}H-NMR spectra were recorded on a Bruker Avance III HD 400 spectrometer equipped with an Ultrashield 9.4 T magnet at 400 MHz.

The **muffle furnace** was a Carbolite CWF1100.

As **pH-meter** a Mettler Toledo SevenMulti and a Mettler Toledo FiveEasy were used. They were calibrated by performing a three point calibration using the standard solutions provided by the manufacturer.

Pure water refers to deionized water from the institute water supply that was purified again using a MilliQ Ultrapure type1 water simplicity UV setup with simplipak2 purification cartridges and a millipak express 20 filter.

Reductions were performed using a "micro effi" system of PID Eng&Tech in a steel fixed bed plug flow reactor.

SEM pictures were taken using a FEI Quanta FEG 250 Scanning Electron Microscope (5 kV accelerating voltage, 10 mm working distance) in high vacuum mode. The sputter coating was performed using a Q150T S sputter coater from Quorum Technologies (Au:Pd 60:40, 30 s, 30 mA).

TPR was performed using a BEL MicrotracBEL Corp. Belcat II. Equilibration time for the TCD was set to 2 h. For MMO catalysts a pre-treatment at 450 °C for 30 min in O_2 was performed. The reduction was performed using 10 % H_2 in Ar heating up to 600 °C with a rate of 5 °C min^{-1}.

The **tubular furnace** setup consisted of an oven (Euroglas Analytical Instruments Furnace) with a Eurotherm 3200 series PID temperature controller and a gas flow controller (Euroglas Analytical Instruments Control Unit) allowing for N_2 flow. A custom made borosilicate glass tube with ground glass joints on each end was used as reactor, samples were inserted using a ceramic weighing boat.

XPS measurements were performed using a custom-built SPECS XPS spectrometer equipped with a monochromatized Al-K_α X-ray source (μFocus 350). The samples were loaded as powder onto the sample holder using double-sided carbon tape. Charge correction was applied so the adventitious carbon peak was centered at a binding energy of 284.8 eV.

XRD measurements were performed on a Philips Xpert in Bragg-Brentano geometry. The diffractometer was equipped with a Cu LFF X-ray tube operated at 45 kV and 40 mA (Cu-K_α), and a BBHD mirror. A previously established standard measurement method was used. The 2θ ranges were set between 20° to 80°.

6.4 Analytical protocols

6.4.1 Washing steps for glass syringe

Washing steps for glass syringes (Hamilton®) were implemented to avoid cross-contamination of samples. Fully wash syringe: Aspirate solvent completely, discharge into beaker or tissue in fumehood. Partially wash syringe: Aspirate solvent until liquid level higher than what was previously in syringe, then pull plunger up completely to rapidly aspirate liquid to 500 µL mark, then discharge into beaker or tissue in fumehood.

6.4.2 Sample preparation for GC analysis

For reporting of conversions and yields a standard method of sample preparation was developed. A 500 µL glass syringe (Hamilton®) was used for liquid transfer. The syringe was washed fully once. 800 µL of solvent were injected into a closed GC vial. 100 µL of internal standard were injected. The syringe was washed partially three times and fully once. If necessary, the sample was allowed to adjust to RT and 100 µL of sample were injected. The syringe was washed partially three times and fully once. The screw cap was opened carefully to release pressure after each injection. The GC vial was shaken to ensure mixing of the liquid phases.

6.4.3 Sample preparation for XRD analysis

All samples were ground into a fine powder if necessary. Crystalline silicon tiles were cleaned using iPrOH. The silicon tile was stuck to the sample holder using modeling mass and leveled to the height of the sample holder by pressing it down with a glass slide. Then, 2-4 drops of heptane were placed on the silicon tile. About 3 mg of sample were added into the heptane. The sample holder was moved in circular motions to spread the powder uniformly over the silicon tile and the heptane was allowed to evaporate.

6.4.4 Sample preparation for SEM imaging

A few grains of the target material were stuck to the sample holder using conductive double-sided adhesive carbon tape. The sample holder together with the sample material was then coated with a about 8 nm thick layer of Au:Pd 60:40 with a sputter coater.

6.5 Methods

6.5.1 Coprecipitation of catalysts

For **HT** synthesis the procedure from [49, pp. 76–77] was used. The respective nitrate salts were dissolved in the desired ratio in pure water. 2:1 Mg:Al (or equivalent ratio of 2+ ions, for example 1:1:1 Cu:Mg:Al) with 25 mmol of Al was used. A solution of NaOH and Na_2CO_3 in pure water was made (2 M NaOH, 0.5 M Na_2CO_3). A beaker was charged with 100 mL of pure water. A calibrated pH-Meter and two burettes were prepared.

One burette was filled with the basic solution and the other one with the metal salt solution. Under magnetic stirring the metal salt solution was added dropwise into the beaker while monitoring the pH in real-time. Base was then added so that the pH was as close as possible around pH 10 throughout the precipitation. It is expected that in the beginning the pH will be very sensitive to addition of base/acid and fluctuate a lot. This stabilized over time of the synthesis. Alternatively, when no 2 burettes were available, the base burette was replaced by manual addition of base via syringe.

The precipitated HT was then collected via filtration. In case filtration was not possible, centrifugation was used. The precipitate was then washed either on a buchner funnel or by repeated centrifugation with pure water until the washing liquid was neutral according to pH paper to remove possible Na^+ contamination.

When washing via centrifugation it is expected that it will become harder to centrifuge the more neutral the solution becomes. The washing process was then stopped when it was noticed that not all of the product could be collected anymore. The product was then dried in a drying oven at 80 °C to 100 °C overnight and ground into a fine powder.

For **MgO** synthesis $Mg(NO_3)_2 \cdot 6\,H_2O$ was precipitated using 2 M NaOH, washed by centrifugation with pure water until neutral on pH paper and then the liquid phase was evaporated at 95 °C on a hotplate, because the precipitate could not be collected by either filtration or centrifugation. The still wet product was dried further at 80 °C in a drying oven.

6.5.2 Calcination of catalysts

HT catalysts were converted to MMO by calcining them at 450 °C for 4 h in a ceramic crucible using a muffle furnace. The **MgO** catalyst was calcined at 450 °C for 2 h.

Spinel catalysts were prepared by thermal decomposition. The respective metal nitrates were dissolved in pure water to ensure homogeneous distribution of the metal ions. The water was then evaporated on a hotplate. The solids were transferred to a tubular furnace connected to the ventilation system and pre-calcined at 450 °C under N_2-flow until no more off-gassing of nitrous gases was noticed. After that, the powder was transferred to a crucible and the final calcination was performed in a muffle furnace. Co-Al-spinel was calcined at 500 °C for 2 h, while the Mg-Al-spinel was calcined at 950 °C for 2 h.

MMO for rehydration experiments were prepared according to the standard method of the research group of David Kubička (Department of Sustainable Fuels and Green Chemistry, UCT Prague). The HT was put in a muffle furnace with a ramp of 3 °C min^{-1} up to 450 °C. That temperature was held for 3 h.

6.5.3 Ex-situ rehydration of catalysts

Rehydration experiments were performed according to the standard procedure provided by the research group of David Kubička (Department of Sustainable Fuels and Green Chemistry, UCT Prague) with adaptions made for the existing laboratory infrastructure. About 50 mg of freshly calcined catalyst was weighed into a glass vial and about 1.3 mL of pure water were added. The vial was shaken shortly, then the material was soaked in the liquid phase without stirring. In case the rehydration was performed at elevated temperatures an aluminum heating block together with a hotplate with a temperature probe was used to regulate the temperature.

After the rehydration was stopped, the material was collected by centrifugation (5 min, 3260 $\times g$). The material was dried either in air in a drying oven or in an inert atmosphere in a tubular furnace under a N_2 flow of 10 mL min^{-1} and afterwards stored under N_2.

6.5.4 Ex-situ reduction of catalysts

The reduction of copper-containing catalysts was performed in a gas flow reactor. The steel reactor tube was prepared by putting in glass wool first, then the powder was added. The reactor tube was connected to the reactor box equipped with an oven and a temperature probe inside the reactor tube. The reduction procedure is described in Table 16 and was performed at atmospheric pressure.

Table 16: Temperature profile and gas flows during reductions of copper-containing MMOs.

Time / min	Temperature / °C	He-flow / 10 mL min^{-1}	H_2-flow / 10 mL min^{-1}
30	30	50	-
37	400	-	10
60	400	-	5
120	-	5	-

After cooling down, the reactor was kept under He atmosphere overnight. When opening the reactor the reduced material was poured into a glass dish where some of the material underwent reoxidation. The reoxidizing material had to be quickly separated physically from the rest of the material to prevent further chain reactions.

6.5.5 Preliminary tests using NaOH

Preliminary tests for batch reactions were performed in glass vials and stirred magnetically. In case BZ was used, a 0.2 M solution in acetone was prepared. NaOH pearls were used as reference catalyst.

A Cannizzaro reaction was performed using neat BZ and NaOH. After 20 min the liquid vanished while the NaOH agglomerated and was discolored yellow. The solids were extracted using EtOH, the extract was measured via GC.

Preliminary flow reactions were performed using a quartz glass tube that was filled with Na_2CO_3, NaOH and Na_2CO_3 again, each section separated by glass wool. 0.2 M BZ solution in acetone was pumped through with a peristaltic pump (ISM831C, Ismatec). Another setup was tested by pushing acetone through a 1 mL syringe (B Braun Inject-F 0.01 mL - 1 mL) packed with the same sections.

6.5.6 Batch reactions

The batch reactions were performed in a highly controlled environment by using a steel reactor (300 mL Series 4760 Pressure Vessel, Parr Instrument Company) equipped with a temperature probe, a rupture disk and a pressure gauge. A PTFE insert was used as well as PTFE coated stirbars (3 cm).

0.5 g of catalyst and 100 mL of reaction mixture were added into the PTFE insert and the reactor. That level of liquid ensured that the temperature probe was measuring the temperature of the reaction mixture and not of the atmosphere inside. The reactor was closed using a wrench. When applicable, heating was started and the reaction time was started as soon as the reaction temperature was reached. The reaction was stirred at 460 rpm using a IKA C-MAG HS 7 digital magnetic stirrer.

Usually, some overshoot of the temperature was recorded (see section 7.4). Since the experiments were performed over a longer period of time (if not noted otherwise, 4 h), that overshoot was assumed to not affect the catalytic activity and tolerated, especially because the pattern was consistent for each reaction.

After the end of the reaction the reactor was allowed to cool down below the boiling temperature of the solvent, opened and immediately a sample was drawn using a syringe. That sample was filtered using a CHROMAFIL Xtra PTFE-20/25 syringe filter (pore size 0.2 µm) into a glass GC vial for further analysis.

In case the used catalyst was of interest, it was collected by gravity filtration and washing with solvent. If the exact composition of the adsorbed organic matter was not of interest, another alternative used was collection by decanting the reaction mixture and evaporation of the solvent.

6.5.7 Flow reactions

The execution of flow reactions followed a standard procedure that was adapted to the specific reaction performed.

First, all lines were cleaned by flushing them with the solvent used in the reaction and dried in a drying oven. The catalyst was sieved to achieve a fraction between 63 µm and 500 µm.

The CatCart was closed on one side by placing an O-ring, the steel filter and the rubber sealing on the opening. Then, the rubber sealing was pressed into its place using the designated press. Catalyst was filled into the CatCart and the other side was sealed in the same manner as described before.

After sealing the CatCart and putting it into its holder, the holder was screwed shut using hBN in acetone as lubricant for the screw thread. All lines were assembled. A pressure test was performed by pressurizing the system up to the maximum pressure and flow rate that would be used in the experiment already using the respective gas. In case H_2 was the gas phase in the experiment, first a pressure test with inert gas was performed to detect major leaks. If H_2 was used, connections that could potentially cause leaks were further monitored by placing a CO/H_2 sensor near the connection. In case a leak was detected or the desired pressure could not be reached, faulty connections were replaced.

The feed was prepared and connected to the HPLC pump; if necessary the line was preflushed with solvent to remove air bubbles. If required, an in-situ pre-treatment of the catalyst was performed. For this, the CatCart was placed inside the oven.

For aldol condensations the pre-treatment consisted of heating to 250 °C at a rate of $10\,°C\,min^{-1}$ while flowing O_2 at a rate of $10\,mL\,min^{-1}$ with a backpressure of 10 bar. For hydrogenation reactions the reactor was also heated to 250 °C at a rate of $10\,°C\,min^{-1}$ while flowing H_2 at a rate of $10\,mL\,min^{-1}$ with a backpressure of 20 bar. In both cases, temperature, gas flow and pressure were held for 1 h.

After the pre-treatment the CatCart was allowed to cool to reaction temperature. When the reaction was performed at RT, the CatCart was placed outside of the oven to ease the monitoring for leaks.

During normal operation of the flow reactor, the liquid feed was pumped through the system at $0.1\,mL\,min^{-1}$ into a waste flask that was sealed except for tubing connecting to the ventilation system. The breakthrough time depended on the exact setup used, but usually was between 1 h to 2 h of operation.

For taking samples, the flow could be switched from the waste flask to another tubing that was first flushed into a waste beaker to remove old reaction mixture. Meanwhile, a GC vial was covered with parafilm and placed onto ice to minimize evaporation of solvent. The tubing was stuck through the parafilm and sample was collected. After reaching the desired amount of sample, the product stream was switched again to the waste flask.

To stop the reaction, the remaining liquid was pushed out by flowing gas (O_2 for aldol condensations, inert gas for hydrogenations) until there was no liquid coming

out anymore (visual control). The lines connecting to the CatCart as well as the CatCart itself were disassembled and cleaned. When of interest, the catalyst inside the CatCart was recovered and stored.

Wherever deviations of those standard operating procedures were realized, it is specified in the respective results and discussion section.

In case of reactions with MMO as catalyst, the catalyst was pre-treated by calcining at 450 °C for 30 min in a muffle oven. For aldol condensations, it was used as close to 350 mg of catalyst as possible, while for the hydrogenation reactions due to the lower powder density of the catalysts the target amount was 170 mg.

6.6 Syntheses

6.6.1 1,5-Diphenyl-1,4-pentadiene-3-one (dibenzylideneacetone, dba)

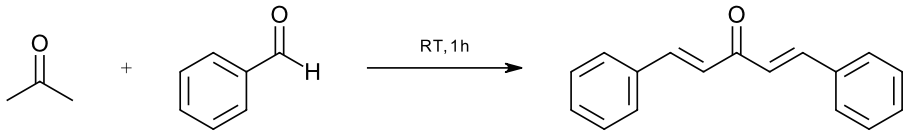

Figure 39: Overview of the synthesis of dba.

Table 17: Reagents used for the synthesis of dba. Directly measured values are highlighted in bold.

	M / g mol^{-1}	m / g	V / mL	n / mmol	eq / 1
Acetone	58.08	1.2	**1.6**	21	1.0
Benzaldehyde	106.13	5.0	**4.8**	47	2.2
EtOH	-	-	**25**	-	-
NaOH in water	-	**2**	**20**	-	-

Dba was prepared following the procedure from [50]. Benzaldehyde and acetone were dissolved in EtOH. NaOH solution was added over 1 min, immediately turning the solution yellow. After the addition of 10 mL of NaOH solution a yellow precipitate formed. After 1 h of stirring magnetically at RT, the reaction mixture was poured into water. The solids were filtered off and washed with water. A yellow powder was obtained. It was predried for 20 min on the filter using vacuum. GC analysis showed that the crude consisted of mostly one product. The crude product was stored for further workup.

Yield (% of theory, crude): 93
^{1}H NMR (400 MHz, Chloroform-d) δ 10.03 (s, 0H), **7.74 (d, J = 15.9 Hz, 2H), 7.66 – 7.59 (m, 4H), 7.45 – 7.39 (m, 6H), 7.09 (d, J = 16.0 Hz, 2H)**, 4.83 – 4.74 (m, 13H), 3.78 – 3.67 (m, 1H), 1.63 (s, 7H), 1.32 – 1.21 (m, 3H).
Marked **fat** corresponds to product. [51]

Impurities identified: δ 10.03 (unreacted BZ), 1.63 (water), 1.32-1.21/3.78-3.67 (EtOH)
GC-purity (% based on area-%): 70

6.6.2 1,5-Di-2-furanyl-1,4-pentadien-3-one (difurfurylideneacetone, F2con)

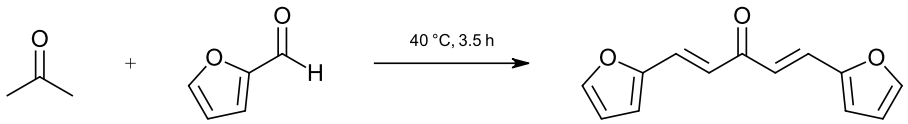

Figure 40: Overview of the synthesis of F2con.

Table 18: Reagents used for the synthesis of F2con. Directly measured values are highlighted in bold.

	M / g mol^{-1}	m / g	V / mL	n / mmol	eq / 1
Acetone	58.08	3.9	**4.9**	66.6	1.0
Furfural	96.08	12.8	**11.0**	133	2.0
NaOH	-	**1**	**-**	-	-
DI water	-	-	**50**	-	-

F2con was synthesized according to [49, p. 214]. NaOH was dissolved in DI water. Acetone was added, turning the solution cloudy. Upon the addtion of furfural a yellow solid started precipitating. The reaction mixture was heated to 40 °C in a water bath and stirred magnetically for 3.5 h, then allowed to cool to RT and stored overnight. After presumed completion of the reaction it was cooled down using an ice bath for 3 h. The precipitate was collected via filtration and a mix of brown solid and yellow crystals was obtained. The crude was stored for further workup.

Yield (% of theory, crude): 225
GC-purity (% based on area-%): 95

7 Supporting information

7.1 Reliability of BET surface area measurements

The robustness of BET surface area measurements was tested by performing repeated measurements with different amounts of the same material. The results shown in Table 19 indicate good robustness, therefore in case it was necessary to use more or less material for experimental reasons than in the standard method using 0.1 g, BET surface area measurements were performed and reported as usual.

Table 19: Results of BET surface area measurements with different amounts of the same material.

Mass (approximate) / g	BET surface area / $m^2\,g^{-1}$
0.1	61.228
1	61.192

7.2 GC - method development

7.2.1 aldol_acetone_benzaldehyde_320C

A standard ramp from 60 °C to 320 °C was the starting point of method development. The starting temperature was lowered to 40 °C to help separation of low-boiling compounds. A prolonged holding time of 30 min at 320 °C was tried to see if there are late eluting compounds in the mixture. As there were no peaks at a retention time of 20 min or later after several reactions, the method was cut off at 20 min. This gradient is shown in Table 20

Table 20: Temperature gradient of method aldol_acetone_benzaldehyde_320C.

Rate / °C min^{-1}	Temperature / °C	Hold time / min
-	40	7
50	320	7.4

A calibration using BZ, DAA and MES standards was tried. However, it was found that the repeatability between injections was too low, giving deviations of up to 50 % compared to the true value of validation standards. To counter this problem, an internal standard was searched for. Trans-cinnamic acid, biphenyl, hydroquinone and benzophenone were tried as internal standard. Benzophenone was determined as the best option, giving a sharp signal not overlapping with any other peaks that were expected in the reaction mixture.

7.2.2 aldol_320C_2024-04-23

With the previously described method, separation of BZcon and the unknown product was not possible. To enable better quantification of benzylideneacetone, the

method was further optimized for better separation and shorter runtimes until baseline separation of all starting material and product peaks was possible. The optimized temperature program is shown in Table 21.

Table 21: Temperature gradient of method aldol_320C_2024-04-23.

Rate / °C min^{-1}	Temperature / °C	Hold time / min
-	40	2
50	150	3
50	320	4.4

7.3 GC - calibration and validation

7.3.1 Linear range

The goal of analysis was to provide quantitative data for batch and flow reaction experiments of aldol condensations. For this target a minimum linear range of 3 orders of magnitude was expected to be sufficient. To determine the working range of the instrument, linearity for BZ, DAA and MES was tested over 6 orders of magnitude. Since the starting concentration of BZ was constant in all experiments (about 0.2 mmol mL^{-1}), the highest standard was chosen in that concentration range.

The results of that test can be seen in Figure 41. MES could not be detected in the lowest concentration. For BZ the lowest standard does also not give a linear response anymore. For DAA the area aproaches a constant value of about $1 \cdot 10^5$, which was attributed to the presence of DAA in the acetone solvent. Subtracting the area of DAA of a blank measurement of acetone leads to improved linearity. However, it was decided that the baseline presence of acetone in the samples would be accepted and the results would not be corrected mathematically.

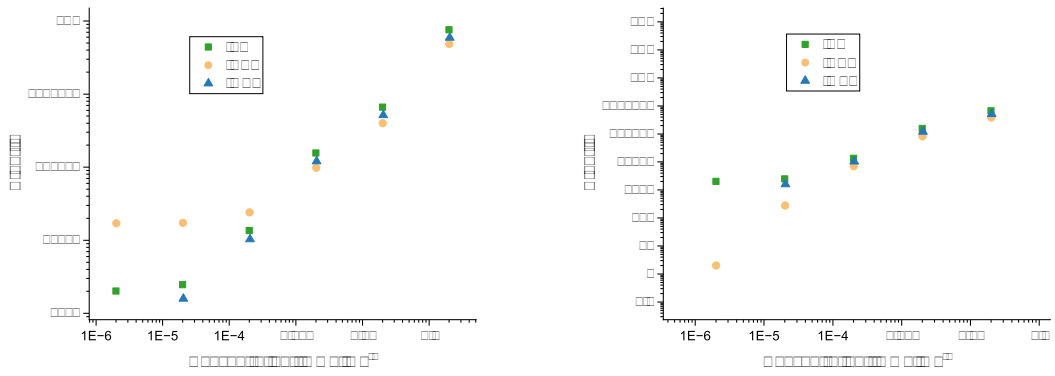

(a) (b)

Figure 41: Area over concentration plotted for standard measurements of BZ, DAA and MES over a concentration range from 0.1 mmol mL^{-1} to $1 \cdot 10^{-6}$ mmol mL^{-1} (a) without and (b) with DAA blank subtracted.

Since the highest standards were prone to fronting, presumably from column overload, it was decided to dilute samples 1:10 to retain good separation of samples with more analytes. A higher dilution was dismissed to avoid problems with interference from baseline DAA in acetone.

7.3.2 Calibration

For the calibration shown in Figure 42 6 points were chosen spaced equally over the range of interest (1 % to 100 % for BZ and BZcon, DAA and MES were chosen in the same concentration range because of experience from previous analyses). For the second calibration one standard was excluded because of mistakes in preparation, which can be seen in Figure 42 (b) and (c).

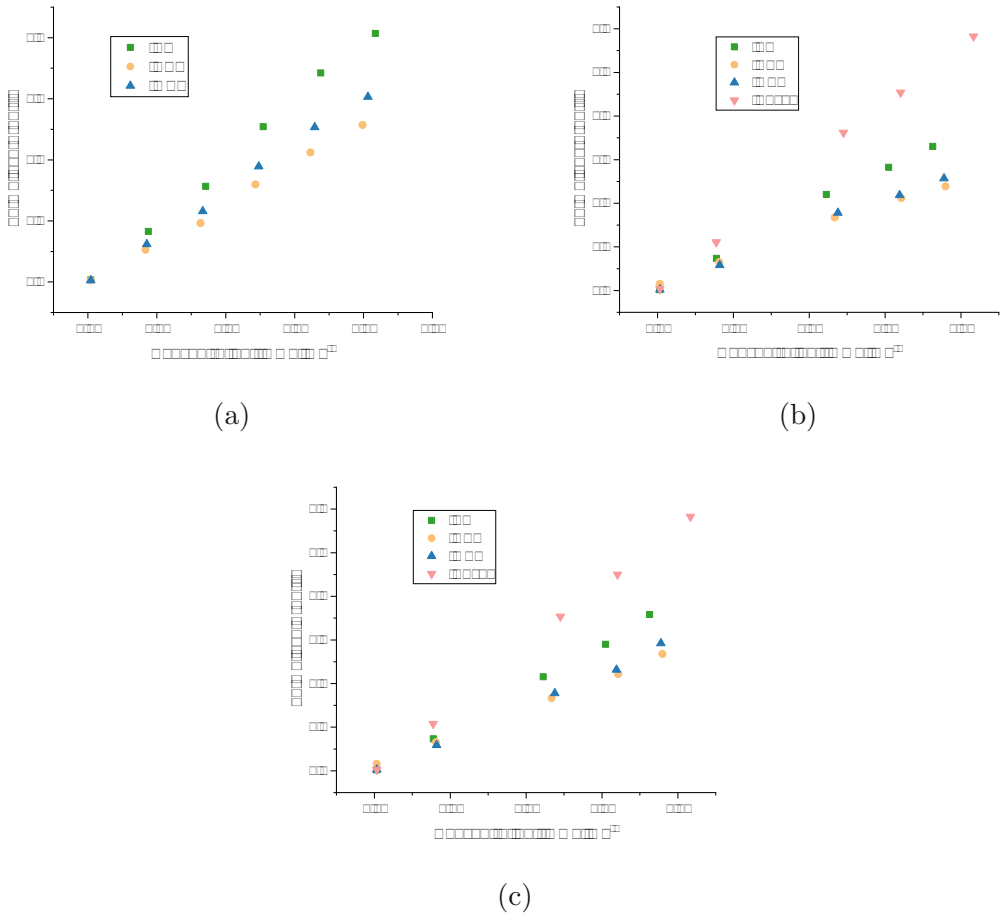

(a) (b)

(c)

Figure 42: Calibration curves for (a) method section 7.2.1, 2024-04-15 (b) method section 7.2.1, 2024-06-18 (c) method section 7.2.2, 2024-06-18.

7.3.3 Validation

Linearity was checked by visual inspection of the fit curve and its residuals.

Independently prepared validation standards with concentrations of about 5 %, 50 % and 95 % of the highest standard were measured for the first calibration. The true-

ness as recovery (percent of the value calculated for the standard) is shown in Table 22.

Table 22: Assessment of trueness of measurements based on recovery of standards throughout the calibration range.

Percent of highest standard / %	Recovery BZ / %	Recovery DAA / %	Recovery MES / %
5	113	119	116
50	102	99	101
95	99	96	97

The deviation from the calculated value of mostly $< 5\,\%$ was deemed acceptable. Samples at the lower range of calibration have higher relative deviation. However, the absolute error at those concentrations was assessed as small enough for the purpose of measuring yields and conversions.

The GC method showed good repeatability as seen in Table 23.

Table 23: Repeatability of the GC method based on 6 measurements. It should be highlighted that those numbers do not quantify the repeatability of the measurement method, as the standards were not independently prepared.

	BZ	DAA	MES
Mean / $\mathrm{mmol\,mL^{-1}}$	0.011365	0.011150	0.011368
s / $\mathrm{mmol\,mL^{-1}}$	$5.17 \cdot 10^{-5}$	$1.68 \cdot 10^{-4}$	$1.24 \cdot 10^{-4}$

LOD and LOD were determined using a method described in [52]. Since no specific measurements were performed to determine LOD/LOQ, the method using only parameters available from the calibration curve was chosen. Therefore, s was determined as standard error of the Y-intercept of the calibration curve. The respective formulas are shown in equation 2 and 3.

$$LOD = 3.3 \cdot \frac{s}{b} \tag{2}$$

$$LOQ = 10 \cdot \frac{s}{b} \tag{3}$$

LOD and LOQ for all compounds intended for quantification are reported in Table 24 for all calibrations used.

Table 24: LOD and LOQ for all substances intended for quantitative analysis and all calibrations.

2024-04-15	BZ	DAA	MES	Bzcon
LOD / mmol mL^{-1}	0.0095	0.0092	0.0089	-
LOQ / mmol mL^{-1}	0.0287	0.0279	0.0271	-
2024-06-18				
LOD / mmol mL^{-1}	0.0117	0.0155	0.0151	0.0084
LOQ / mmol mL^{-1}	0.0355	0.0469	0.0459	0.0253
2024-06-18 short				
LOD / mmol mL^{-1}	0.0063	0.0060	0.0115	0.0052
LOQ / mmol mL^{-1}	0.0191	0.0181	0.0350	0.0158

When reporting quantitative GC results it is stated if they are below the LOD/LOQ, however, for better visualization of results the calculated numbers are nonetheless reported in brackets.

7.3.4 Equivalency of calibrations for quantification

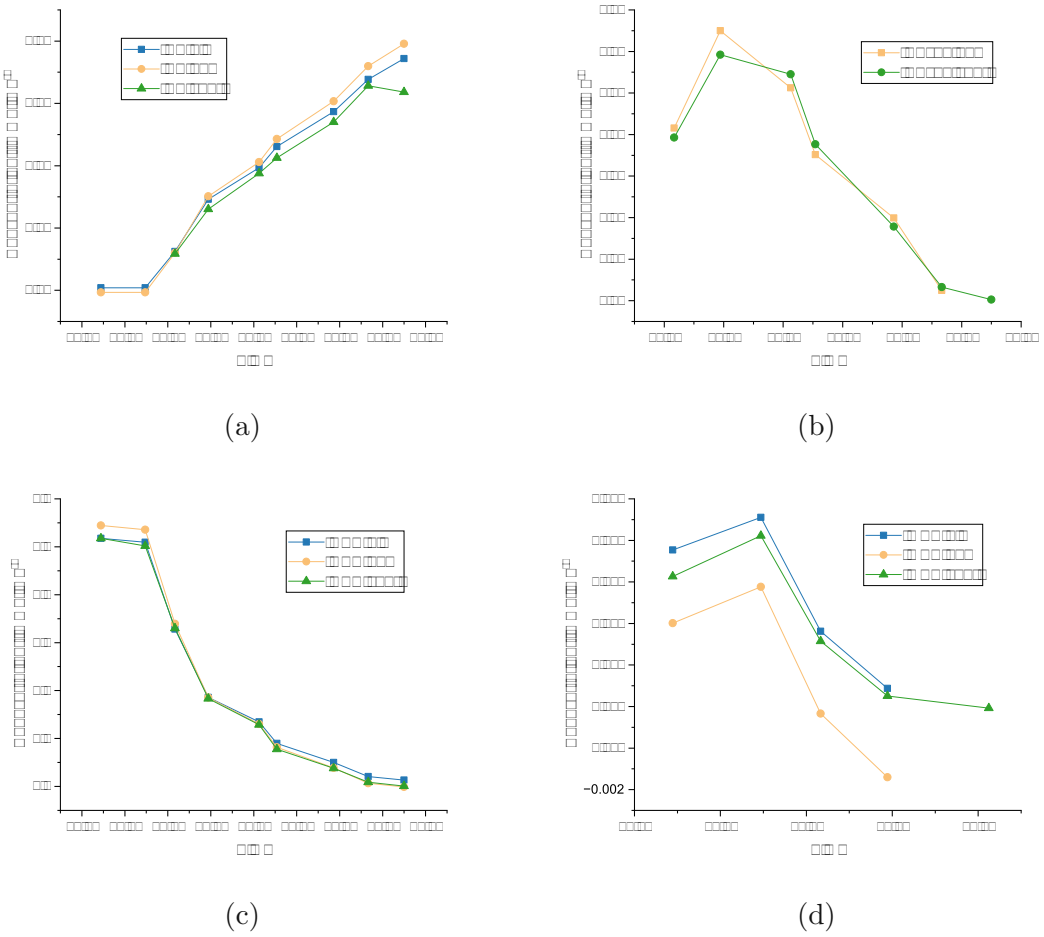

(a) (b) (c) (d)

Figure 43: Analytes of exemplary aldol condensation flow reaction plotted for different calibrations. 'Old' refers to calibration from 2024-04-15 performed with method 'aldol_acetone_benzaldehyde_320C'. 'New' refers to calibration from 2024-06-18 performed with method 'aldol_320C_2024-04-23'. 'Short' refers to calibration from 2024-06-18 performed with method 'aldol_320C_2024-04-23'.

The different calibrations were plotted (Figure 43) for the same flow reaction to examine their equivalency. Good agreement of the trend of the concentration between all three was ascertained, therefore the results are viewed as equal for the purpose of this thesis. One exception is the last datapoint in 43 (a) (BZ short). As the calibration of the other components do not have that outlier it was assumed to be a one-time off event.

7.4 Heating profile of acetone solutions in the batch reactor

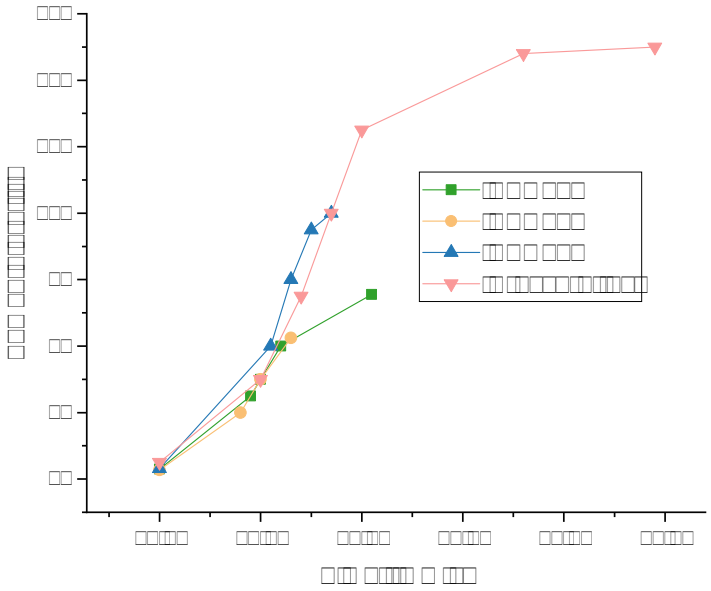

Figure 44: Heating profile of acetone solutions in the batch reactor. For AED020 and AED021 the set temperature was 60 °C, for AED024 the set temperature was 100 °C and for the pressure test the set temperature was 150 °C.

When considering the heating profile of the batch reactor depicted in Figure 44 low target temperatures up to 100 °C are reached quickly with considerable overshoot of the set temperature. Since the time heating up is small in comparison to the total reaction time (4 h) and very consistent between reactions, the starting time of the reaction was defined to be the time where the temperature reached the target temperature.

7.5 Incorporation of remains in dirty crucible into structure

When performing a calcination for $MgAl_2O_4$ spinel synthesis a crucible was used that was stained red from an unknown previous reaction. After the calcination the calcined material took on a slightly red color, while the crucible was less colored than before. When repeating the experiment with a new crucible, no such color change was observed. This points to inclusion of the remains in the old crucible and highlights the importance of using clean equipment to avoid contamination that potentially could alter the surface and therefore the catalytic behavior of material.

7.6 Chromatograms of hydrogenation reactions

In section 3.4 only selected chromatograms of the hydrogenation reactions representative of the main findings were shown due to reasons of readability. The remaining chromatograms are depicted in Figure 45.

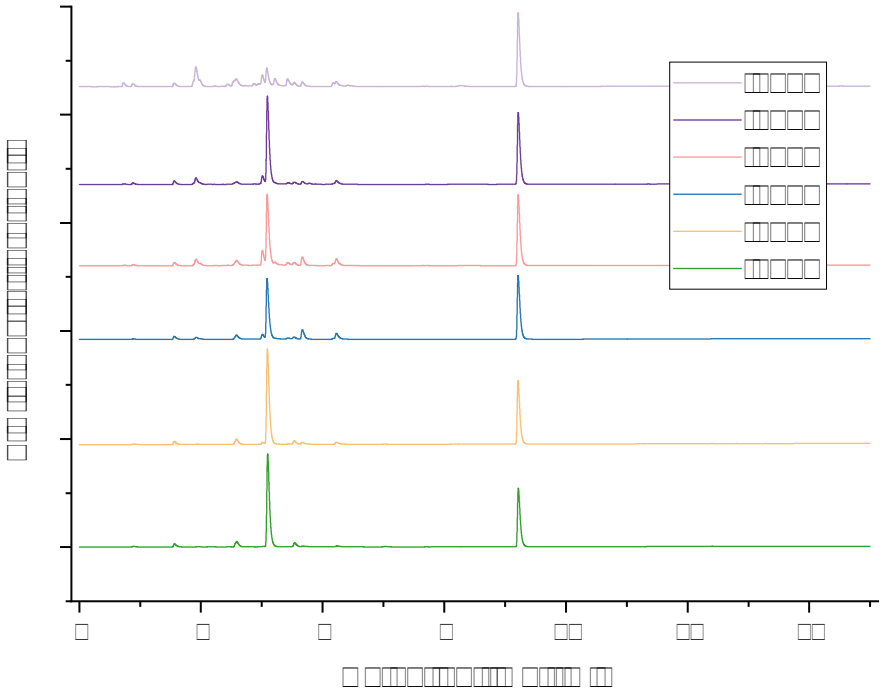

(a)

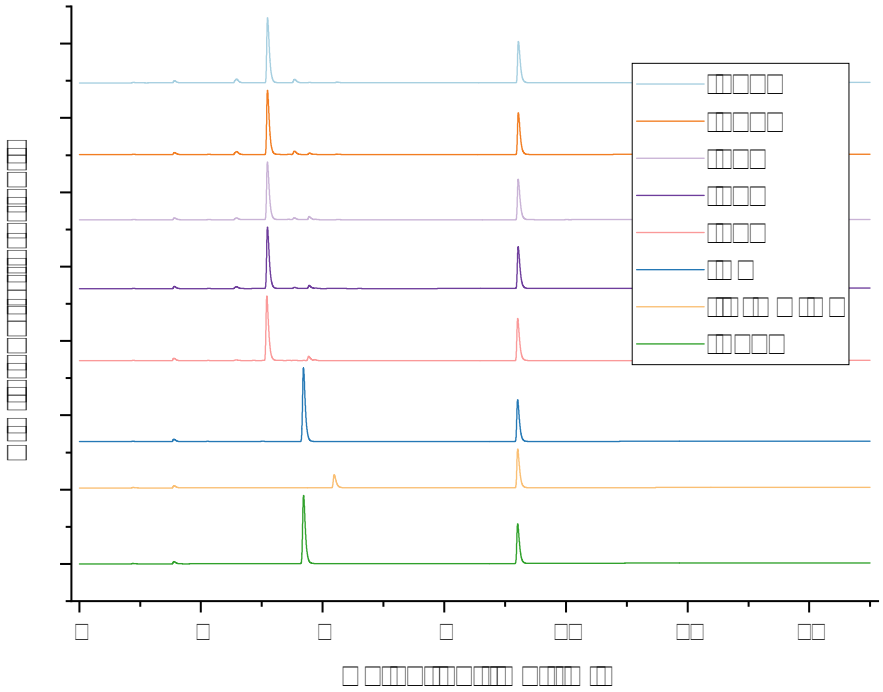

(b)

Figure 45: Chromatograms of hydrogenation reactions of Fcon taken at different temperatures.

7.7 Catalyst preparation scheme

In Figure 46 the relations between the hydrotalcite-derived catalysts are depicted.

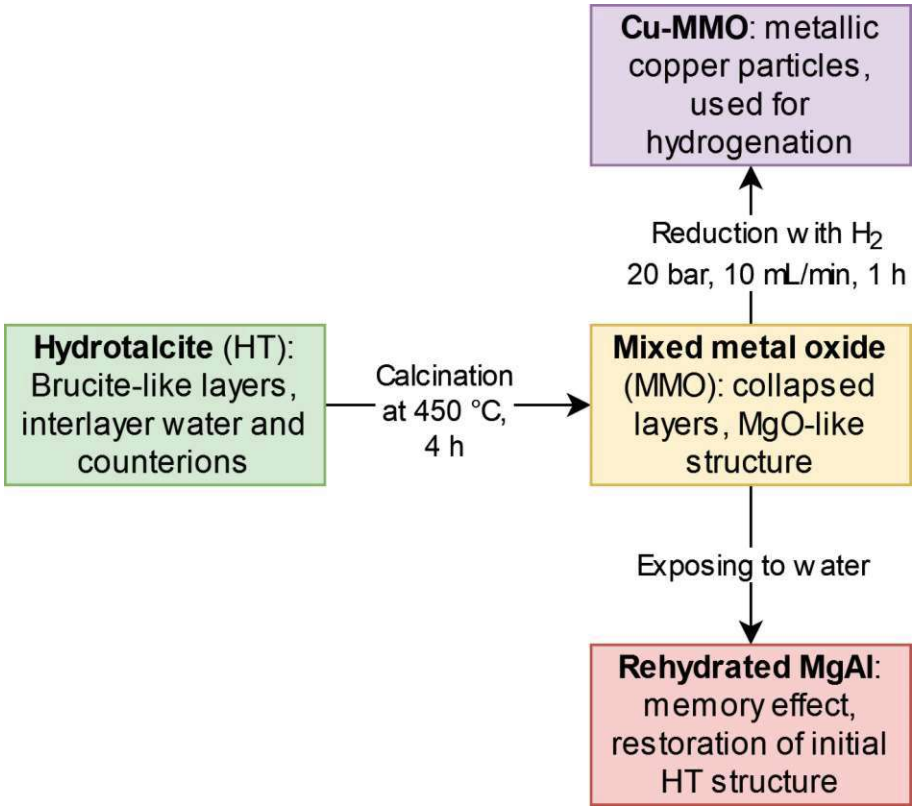

Figure 46: Schematic overview of the hydrotalcite-derived catalysts used in this work.

References

[1] George W. Huber and James A. Dumesic. "An overview of aqueous-phase catalytic processes for production of hydrogen and alkanes in a biorefinery". In: *Catalysis Today*. Frontiers in Catalysis: A Molecular View of Industrial Catalysis 111.1 (Jan. 15, 2006), pp. 119–132. ISSN: 0920-5861. DOI: 10.1016/j.cattod.2005.10.010. URL: https://www.sciencedirect.com/science/article/pii/S0920586105007121 (visited on 08/26/2024).

[2] Hochan Chang et al. "Synthesis of biomass-derived feedstocks for the polymers and fuels industries from 5-(hydroxymethyl)furfural (HMF) and acetone". In: *Green Chemistry* 21.20 (2019). Publisher: Royal Society of Chemistry, pp. 5532–5540. DOI: 10.1039/C9GC01859J. URL: https://pubs.rsc.org/en/content/articlelanding/2019/gc/c9gc01859j (visited on 08/26/2024).

[3] Kottapalli Koteswara Rao et al. "Activation of Mg–Al Hydrotalcite Catalysts for Aldol Condensation Reactions". In: *Journal of Catalysis* 173.1 (Jan. 1, 1998), pp. 115–121. ISSN: 0021-9517. DOI: 10.1006/jcat.1997.1878. URL: https://www.sciencedirect.com/science/article/pii/S0021951797918789 (visited on 08/24/2024).

[4] D. Tichit et al. "Textural Properties and Catalytic Activity of Hydrotalcites". In: *Journal of Catalysis* 151.1 (Jan. 1, 1995), pp. 50–59. ISSN: 0021-9517. DOI: 10.1006/jcat.1995.1007. URL: https://www.sciencedirect.com/science/article/pii/S002195178571007X (visited on 08/26/2024).

[5] Sònia Abelló, D. Vijaya-Shankar, and Javier Pérez-Ramírez. "Stability, reutilization, and scalability of activated hydrotalcites in aldol condensation". In: *Applied Catalysis A: General* 342.1 (June 30, 2008), pp. 119–125. ISSN: 0926-860X. DOI: 10.1016/j.apcata.2008.03.010. URL: https://www.sciencedirect.com/science/article/pii/S0926860X08001634 (visited on 08/26/2024).

[6] Charles L. Perrin and Kuei-Lin Chang. "The Complete Mechanism of an Aldol Condensation". In: *The Journal of Organic Chemistry* 81.13 (July 1, 2016). Publisher: American Chemical Society, pp. 5631–5635. ISSN: 0022-3263. DOI: 10.1021/acs.joc.6b00959. URL: https://doi.org/10.1021/acs.joc.6b00959 (visited on 08/25/2024).

[7] A. Aguilera et al. "Ba(OH)2 as the catalyst in organic reactions. Part XIV. Mechanism of Claisen–Schmidt condensation in solid–liquid conditions". In: *Canadian Journal of Chemistry* 65.6 (June 1987). Publisher: NRC Research Press, pp. 1165–1171. ISSN: 0008-4042. DOI: 10.1139/v87-195. URL: https://cdnsciencepub.com/doi/10.1139/v87-195 (visited on 10/04/2024).

[8] Hideshi Hattori. "Solid base catalysts: generation of basic sites and application to organic synthesis". In: *Applied Catalysis A: General*. Celebration Issue 222.1 (Dec. 20, 2001), pp. 247–259. ISSN: 0926-860X. DOI: 10.1016/S0926-860X(01)00839-0. URL: https://www.sciencedirect.com/science/article/pii/S0926860X01008390 (visited on 10/06/2024).

[9] Joseph D. Gettler and Louis P. Hammett. "Rates and Temperature Coefficients of the Hydroxyl Ion Catalyzed Aldol Condensation of Benzaldehyde with Methyl Ethyl Ketone and Acetone [1]". In: *Journal of the American Chemical Society* 65.10 (Oct. 1943), pp. 1824–1829. ISSN: 0002-7863, 1520-5126. DOI: 10.1021/ja01250a010. URL: https://pubs.acs.org/doi/abs/10.1021/ja01250a010 (visited on 10/06/2024).

[10] Swagata Mandal et al. "Review of the aldol reaction". In: *Synthetic Communications* 46.16 (Aug. 17, 2016). Publisher: Taylor & Francis _eprint: https://doi.org/10.1080/00397911.2016.1206938, pp. 1327–1342. ISSN: 0039-7911. DOI: 10.1080/00397911.2016.1206938. URL: https://doi.org/10.1080/00397911.2016.1206938 (visited on 10/06/2024).

[11] Savita Bargujar and Sonia Ratnani. "An Alternative Greener Synthesis of Dibenzalacetone". In: *Organic Preparations and Procedures International* 54.6 (Nov. 2, 2022). Publisher: Taylor & Francis _eprint: https://doi.org/10.1080/00304948.2022.2096383, pp. 563–565. ISSN: 0030-4948. DOI: 10.1080/00304948.2022.2096383. URL: https://doi.org/10.1080/00304948.2022.2096383 (visited on 10/06/2024).

[12] Sk Manirul Islam et al. "Graphene based material as a base catalyst for solvent free Aldol condensation and Knoevenagel reaction at room temperature". In: *Journal of Molecular Catalysis A: Chemical* 394 (Nov. 15, 2014), pp. 66–73. ISSN: 1381-1169. DOI: 10.1016/j.molcata.2014.06.038. URL: https://www.sciencedirect.com/science/article/pii/S1381116914002891 (visited on 10/06/2024).

[13] Craig M. Comisar and Phillip E. Savage. "Kinetics of crossed aldol condensations in high-temperature water". In: *Green Chemistry* 6.4 (Apr. 14, 2004). Publisher: The Royal Society of Chemistry, pp. 227–231. ISSN: 1463-9270. DOI: 10.1039/B314622G. URL: https://pubs.rsc.org/en/content/articlelanding/2004/gc/b314622g (visited on 10/06/2024).

[14] Nurul A. Mazumder and Ruma Rano. "An efficient solid base catalyst from coal combustion fly ash for green synthesis of dibenzylideneacetone". In: *Journal of Industrial and Engineering Chemistry* 29 (Sept. 25, 2015), pp. 359–365. ISSN: 1226-086X. DOI: 10.1016/j.jiec.2015.04.015. URL: https://www.sciencedirect.com/science/article/pii/S1226086X15001446 (visited on 10/06/2024).

[15] Jennifer D. Lewis, Stijn Van de Vyver, and Yuriy Román-Leshkov. "Acid–Base Pairs in Lewis Acidic Zeolites Promote Direct Aldol Reactions by Soft Enolization". In: *Angewandte Chemie International Edition* 54.34 (2015). _eprint: https://onlinelibrary.wiley.com/doi/pdf/10.1002/anie.201502939, pp. 9835–9838. ISSN: 1521-3773. DOI: 10.1002/anie.201502939. URL: https://onlinelibrary.wiley.com/doi/abs/10.1002/anie.201502939 (visited on 10/18/2024).

[16] Yuhang Wang et al. “Tuning of CO $_2$ Reduction Selectivity on Metal Electrocatalysts”. In: *Small* 13.43 (Nov. 2017), p. 1701809. ISSN: 16136810. DOI: 10.1002/smll.201701809. URL: https://onlinelibrary.wiley.com/doi/10.1002/smll.201701809 (visited on 01/10/2022).

[17] Alain Guida et al. “Hydrotalcites as base catalysts. Kinetics of Claisen-Schmidt condensation, intramolecular condensation of acetonylacetone and synthesis of chalcone”. In: *Applied Catalysis A: General* 164.1 (Dec. 23, 1997), pp. 251–264. ISSN: 0926-860X. DOI: 10.1016/S0926-860X(97)00175-0. URL: https://www.sciencedirect.com/science/article/pii/S0926860X97001750 (visited on 10/18/2024).

[18] Iva Paterová, Eliška Vyskočilová, and Libor Červený. “Two-Step Preparation of Benzylacetone”. In: *Topics in Catalysis* 55.11 (Aug. 1, 2012), pp. 873–879. ISSN: 1572-9028. DOI: 10.1007/s11244-012-9853-8. URL: https://doi.org/10.1007/s11244-012-9853-8 (visited on 10/06/2024).

[19] L. Guczi, Á. Molnár, and D. Teschner. “7.16 - Hydrogenation Reactions: Concepts and Practice”. In: *Comprehensive Inorganic Chemistry II (Second Edition)*. Ed. by Jan Reedijk and Kenneth Poeppelmeier. Amsterdam: Elsevier, Jan. 1, 2013, pp. 421–457. ISBN: 978-0-08-096529-1. DOI: 10.1016/B978-0-08-097774-4.00713-0. URL: https://www.sciencedirect.com/science/article/pii/B9780080977744007130 (visited on 08/27/2024).

[20] John S. Carey et al. “Analysis of the reactions used for the preparation of drug candidate molecules”. In: *Organic & Biomolecular Chemistry* 4.12 (June 8, 2006). Publisher: The Royal Society of Chemistry, pp. 2337–2347. ISSN: 1477-0539. DOI: 10.1039/B602413K. URL: https://pubs.rsc.org/en/content/articlelanding/2006/ob/b602413k (visited on 08/27/2024).

[21] Tim Luttrell et al. “Why is anatase a better photocatalyst than rutile? - Model studies on epitaxial TiO2 films”. In: *Scientific Reports* 4.1 (Feb. 10, 2014). Number: 1 Publisher: Nature Publishing Group, p. 4043. ISSN: 2045-2322. DOI: 10.1038/srep04043. URL: https://www.nature.com/articles/srep04043 (visited on 05/15/2023).

[22] Jia-qi Bai et al. “Efficient NiIr alloy catalyst for selective hydrogenation of benzonitrile, crotonaldehyde and benzylideneacetone”. In: *Catalysis Communications* 176 (Mar. 1, 2023), p. 106630. ISSN: 1566-7367. DOI: 10.1016/j.catcom.2023.106630. URL: https://www.sciencedirect.com/science/article/pii/S1566736723000328 (visited on 08/27/2024).

[23] Katia Martina et al. “Copper-Catalyzed Continuous-Flow Transfer Hydrogenation of Nitroarenes to Anilines: A Scalable and Reliable Protocol”. In: *Organic Process Research & Development* 28.5 (May 17, 2024). Publisher: American Chemical Society, pp. 1515–1528. ISSN: 1083-6160. DOI: 10.1021/acs.oprd.3c00144. URL: https://doi.org/10.1021/acs.oprd.3c00144 (visited on 08/27/2024).

[24] J. T. Wehrli et al. “Selective hydrogenation of propyne over an ion-exchanged copper on silica catalyst”. In: *Applied Catalysis* 66.1 (Nov. 5, 1990), pp. 199–208. ISSN: 0166-9834. DOI: 10.1016/S0166-9834(00)81638-3. URL: https://www.sciencedirect.com/science/article/pii/S0166983400816383 (visited on 08/27/2024).

[25] Blaise Bridier, Núria López, and Javier Pérez-Ramírez. “Partial hydrogenation of propyne over copper-based catalysts and comparison with nickel-based analogues”. In: *Journal of Catalysis* 269.1 (Jan. 1, 2010), pp. 80–92. ISSN: 0021-9517. DOI: 10.1016/j.jcat.2009.10.019. URL: https://www.sciencedirect.com/science/article/pii/S0021951709003637 (visited on 08/27/2024).

[26] Kasanneni Tirumala Venkateswara Rao et al. “Green synthesis of heterogeneous copper-alumina catalyst for selective hydrogenation of pure and biomass-derived 5-hydroxymethylfurfural to 2,5-bis(hydroxymethyl)furan”. In: *Applied Catalysis A: General* 609 (Jan. 5, 2021), p. 117892. ISSN: 0926-860X. DOI: 10.1016/j.apcata.2020.117892. URL: https://www.sciencedirect.com/science/article/pii/S0926860X20304853 (visited on 08/27/2024).

[27] Roberto Spogliarich et al. “Selective hydrogenation of benzylideneacetone catalyzed by iridium diphosphine complexes”. In: *Journal of Molecular Catalysis* 50.1 (Feb. 23, 1989), pp. 19–29. ISSN: 0304-5102. DOI: 10.1016/0304-5102(89)80106-3. URL: https://www.sciencedirect.com/science/article/pii/0304510289801063 (visited on 10/06/2024).

[28] Charles A. Mebi and Brian J. Frost. “Effect of pH on the Biphasic Catalytic Hydrogenation of Benzylidene Acetone Using CpRu(PTA)2H”. In: *Organometallics* 24.10 (May 1, 2005). Publisher: American Chemical Society, pp. 2339–2346. ISSN: 0276-7333. DOI: 10.1021/om048987r. URL: https://doi.org/10.1021/om048987r (visited on 10/06/2024).

[29] Aleksandra Perek-Dlugosz et al. “Electrochemical reduction and consumption of 4-phenyl-3-buten-2-one”. In: *Electrochimica Acta* 123 (Mar. 20, 2014), pp. 412–418. ISSN: 0013-4686. DOI: 10.1016/j.electacta.2014.01.048. URL: https://www.sciencedirect.com/science/article/pii/S0013468614001145 (visited on 10/06/2024).

[30] Yuping Li et al. “Hydrogenation and hydrodeoxygenation of difurfurylidene acetone to liquid alkanes over Raney Ni and the supported Pt catalysts”. In: *Applied Energy* 160 (Dec. 15, 2015), pp. 990–998. ISSN: 0306-2619. DOI: 10.1016/j.apenergy.2015.02.077. URL: https://www.sciencedirect.com/science/article/pii/S0306261915002627 (visited on 10/06/2024).

[31] Yuping Li et al. “Application of Raney Ni and Pt/SiO2-ZrO2 Catalysts for Two-step Hydrogenation of Difurfurylidene Acetone to Long-chain Alkanes”. In: *Energy Procedia*. International Conference on Applied Energy, ICAE2014 61 (Jan. 1, 2014), pp. 2412–2415. ISSN: 1876-6102. DOI: 10.1016/j.egypro.2014.12.016. URL: https://www.sciencedirect.com/science/article/pii/S1876610214030458 (visited on 10/06/2024).

[32] Siti Mariyah Ulfa et al. "Structural Properties of Ni/Al2O3 and Cu/Al2O3 Catalyst and its Application for Hydrogenation of Furfurylidene Acetone". In: *Procedia Chemistry*. International Symposium on Applied Chemistry 2015 16 (Jan. 1, 2015), pp. 616–622. ISSN: 1876-6196. DOI: 10.1016/j.proche.2015.12.100. URL: https://www.sciencedirect.com/science/article/pii/S187661961500248X (visited on 10/06/2024).

[33] Andrew L. McKenzie, Christopher T. Fishel, and Robert J. Davis. "Investigation of the surface structure and basic properties of calcined hydrotalcites". In: *Journal of Catalysis* 138.2 (Dec. 1, 1992), pp. 547–561. ISSN: 0021-9517. DOI: 10.1016/0021-9517(92)90306-3. URL: https://www.sciencedirect.com/science/article/pii/0021951792903063 (visited on 08/24/2024).

[34] D Tichit et al. "Aldol condensation of acetone over layered double hydroxides of the meixnerite type". In: *Applied Clay Science* 13.5 (Nov. 1, 1998), pp. 401–415. ISSN: 0169-1317. DOI: 10.1016/S0169-1317(98)00035-0. URL: https://www.sciencedirect.com/science/article/pii/S0169131798000350 (visited on 08/24/2024).

[35] Kiyotomi Kaneda and Tomoo Mizugaki. "Design of high-performance heterogeneous catalysts using hydrotalcite for selective organic transformations". In: *Green Chemistry* 21.6 (Mar. 18, 2019). Publisher: The Royal Society of Chemistry, pp. 1361–1389. ISSN: 1463-9270. DOI: 10.1039/C8GC03391A. URL: https://pubs.rsc.org/en/content/articlelanding/2019/gc/c8gc03391a (visited on 08/27/2024).

[36] Said Arhzaf et al. "Effect of interlayer anions on the catalytic activity of Mg-Al layered double hydroxides for furfural and acetone aldol condensation reaction". In: *Arabian Journal of Chemistry* 17.1 (Jan. 1, 2024), p. 105412. ISSN: 1878-5352. DOI: 10.1016/j.arabjc.2023.105412. URL: https://www.sciencedirect.com/science/article/pii/S1878535223008742 (visited on 08/26/2024).

[37] Antimo Gioiello et al. "Concepts and Optimization Strategies of Experimental Design in Continuous-Flow Processing". In: *Journal of Flow Chemistry* 6.3 (July 1, 2016), pp. 167–180. ISSN: 2063-0212. DOI: 10.1556/1846.2016.00012. URL: https://doi.org/10.1556/1846.2016.00012 (visited on 08/27/2024).

[38] Roger A. Sheldon. "The E Factor: fifteen years on". In: *Green Chemistry* 9.12 (Nov. 22, 2007). Publisher: The Royal Society of Chemistry, pp. 1273–1283. ISSN: 1463-9270. DOI: 10.1039/B713736M. URL: https://pubs.rsc.org/en/content/articlelanding/2007/gc/b713736m (visited on 08/27/2024).

[39] Hikaru G. Jolliffe and Dimitrios I. Gerogiorgis. "Process modelling and simulation for continuous pharmaceutical manufacturing of ibuprofen". In: *Chemical Engineering Research and Design* 97 (May 1, 2015), pp. 175–191. ISSN: 0263-8762. DOI: 10.1016/j.cherd.2014.12.005. URL: https://www.sciencedirect.com/science/article/pii/S0263876214005164 (visited on 08/27/2024).

[40] Renjing Huang et al. "Furfural Upgrading by Aldol Condensation with Ketones over Solid-Base Catalysts". In: *Catalysis Letters* 152.12 (Dec. 1, 2022), pp. 3833–3842. ISSN: 1572-879X. DOI: 10.1007/s10562-022-03960-1. URL: https://doi.org/10.1007/s10562-022-03960-1 (visited on 08/27/2024).

[41] Juana I Di Cosimo and Carlos R Apesteguía. "Study of the catalyst deactivation in the base-catalyzed oligomerization of acetone". In: *Journal of Molecular Catalysis A: Chemical* 130.1 (Mar. 12, 1998), pp. 177–185. ISSN: 1381-1169. DOI: 10.1016/S1381-1169(97)00204-5. URL: https://www.sciencedirect.com/science/article/pii/S1381116997002045 (visited on 08/27/2024).

[42] Matthias Thommes et al. "Physisorption of gases, with special reference to the evaluation of surface area and pore size distribution (IUPAC Technical Report)". In: *Pure and Applied Chemistry* 87.9 (Oct. 1, 2015), pp. 1051–1069. ISSN: 1365-3075, 0033-4545. DOI: 10.1515/pac-2014-1117. URL: https://www.degruyter.com/document/doi/10.1515/pac-2014-1117/html (visited on 10/06/2024).

[43] František Kovanda et al. "Characterization of activated Cu/Mg/Al hydrotalcites and their catalytic activity in toluene combustion". In: *Applied Clay Science*. Conference of the European Clay Group Association "EUROCLAY 1999" 18.1 (Jan. 1, 2001), pp. 71–80. ISSN: 0169-1317. DOI: 10.1016/S0169-1317(00)00032-6. URL: https://www.sciencedirect.com/science/article/pii/S0169131700000326 (visited on 08/27/2024).

[44] Lisardo Nuñez, G. Pilcher, and H. A. Skinner. "Hot-zone reaction calorimetry the enthalpies of formation of copper oxides". In: *The Journal of Chemical Thermodynamics* 1.1 (Jan. 1, 1969), pp. 31–43. ISSN: 0021-9614. DOI: 10.1016/0021-9614(69)90034-2. URL: https://www.sciencedirect.com/science/article/pii/0021961469900342 (visited on 08/29/2024).

[45] micromeritics. *Temperature-Programmed Reduction Using the AutoChem*. URL: https://www.micromeritics.com/Repository/Files/appnote120.pdf (visited on 10/06/2024).

[46] Natpakan Srisawad et al. "Formation of CoAl2O4 Nanoparticles via Low-Temperature Solid-State Reaction of Fine Gibbsite and Cobalt Precursor". In: *Journal of Nanomaterials* 2012.1 (2012). _eprint: https://onlinelibrary.wiley.com/doi/pdf/10.1155/2012/108369, p. 108369. ISSN: 1687-4129. DOI: 10.1155/2012/108369. URL: https://onlinelibrary.wiley.com/doi/abs/10.1155/2012/108369 (visited on 08/17/2024).

[47] Kristina Pupovac and Regina Palkovits. "Cu/MgAl2O4 as Bifunctional Catalyst for Aldol Condensation of 5-Hydroxymethylfurfural and Selective Transfer Hydrogenation". In: *ChemSusChem* 6.11 (2013). _eprint: https://onlinelibrary.wiley.com/doi/pdf/10.1002/cssc.201300414, pp. 2103–2110. ISSN: 1864-564X. DOI: 10.1002/cssc.201300414. URL: https://onlinelibrary.wiley.com/doi/abs/10.1002/cssc.201300414 (visited on 08/27/2024).

[48] E. C. Craven. "The alkaline condensation of acetone". In: *Journal of Applied Chemistry* 13.2 (1963). _eprint: https://onlinelibrary.wiley.com/doi/pdf/10.1002/jctb.5010130205, pp. 71–77. ISSN: 1934-998X. DOI: 10.1002/jctb.5010130205. URL: https://onlinelibrary.wiley.com/doi/abs/10.1002/jctb.5010130205 (visited on 08/24/2024).

[49] Alberto Tampieri. "Catalytic aldol condensations of bio-derived aldehydes and ketones". PhD thesis. Tarragona: Universitat Rovira i Virgili, 2022.

[50] Xiao Liu et al. "Efficient synthesis of trifluoromethylated cyclopentadienes/fulvenes/norbornenes from divinyl ketones". In: *Organic & Biomolecular Chemistry* 11.39 (Sept. 18, 2013). Publisher: The Royal Society of Chemistry, pp. 6703–6706. ISSN: 1477-0539. DOI: 10.1039/C3OB41400K. URL: https://pubs.rsc.org/en/content/articlelanding/2013/ob/c3ob41400k (visited on 08/12/2024).

[51] Zakaria Ait El Caid et al. "Insight into the Corrosion Inhibition of Dibenzylidene Acetone for Carbon Steel in a Sulfuric Acid Environment: Synthesis, Experimental, and Theoretical Studies". In: *Journal of Bio- and Tribo-Corrosion* 10.1 (Jan. 10, 2024), p. 9. ISSN: 2198-4239. DOI: 10.1007/s40735-023-00813-1. URL: https://doi.org/10.1007/s40735-023-00813-1 (visited on 08/28/2024).

[52] Anneli Kruve et al. "Tutorial review on validation of liquid chromatography–mass spectrometry methods: Part II". In: *Analytica Chimica Acta* 870 (Apr. 22, 2015), pp. 8–28. ISSN: 0003-2670. DOI: 10.1016/j.aca.2015.02.016. URL: https://www.sciencedirect.com/science/article/pii/S0003267015001944 (visited on 08/18/2024).